IEEE Access
Multidisciplinary | Rapid Review | Open Access Journal

Received May 5, 2019, accepted May 29, 2019, date of publication June 10, 2019, date of current version June 26, 2019.

Digital Object Identifier 10.1109/ACCESS.2019.2921800

A Power Series Approach for Hybrid-Duplex UAV Communication Systems Under Rician Shadowed Fading

TAN ZHENG HUI ERNEST, A. S. MADHUKUMAR, (Senior Member, IEEE), RAJENDRA PRASAD SIRIGINA, AND ANOOP KUMAR KRISHNA, (Senior Member, IEEE)

[1]Tan Zheng Hui Ernest is with the School of Computer Science and Engineering, Nanyang Technological University, Singapore e-mail: (tanz0119@e.ntu.edu.sg).
[2]A S Madhukumar is with the School of Computer Science and Engineering, Nanyang Technological University, Singapore e-mail: (asmadhukumar@ntu.edu.sg).
[3]Rajendra Prasad Sirigina is with the School of Computer Science and Engineering, Nanyang Technological University, Singapore e-mail: (raje0015@ntu.edu.sg).
[4]Anoop Kumar Krishna is with Airbus Singapore Pte Ltd, Singapore e-mail: (anoopkumar.krishna@airbus.com).

Corresponding author: Tan Zheng Hui Ernest (tanz0119@ntu.edu.sg)

This work was supported by Airbus Singapore Pte Ltd and the Singapore Economic Development Board (EDB).

ABSTRACT A hybrid-duplex (HBD) UAV communication system (UCS), i.e., HBD-UCS, to improve spectrum utilization is investigated in this work. By considering the combined effect of fading and shadowing, a comprehensive outage probability analysis of the HBD-UCS under various inter-UAV interference and shadowing scenarios over Rician shadowed fading channels is conducted. It is demonstrated that the ground station (GS) in full-duplex (FD) mode operates at lower outage probability than in half-duplex (HD) mode. Furthermore, the joint detector is shown to achieve lower outage probability than the interference ignorant (II) detector and HD-UCS, even when severe shadowing is encountered. As such, utilizing joint detectors in an HBD-UCS enables multi-UAV networks to achieve high reliability when operating in urban environments.

INDEX TERMS Unmanned aerial vehicle, spectrum efficiency, half-duplex, full-duplex, hybrid-duplex, outage probability, rician, shadowing.

I. INTRODUCTION

The application of unmanned aerial vehicles (UAVs) has been gaining attention in recent years from both industry and academia, with diverse UAV applications, e.g., telecommunications relaying [1] and sensor data collection for Internet-of-Things [2], noted in the literature. However, individual UAVs are limited by restrictions on payload, flight time, and lack of link redundancy [1], [3], along with size, weight and power constraints [4]. Thus, the development of multi-UAV networks has seen particular interest in the literature to overcome the limitation of single-UAV applications while maximizing the coverage and functionality of UAVs [3].

A. MOTIVATION AND RELATED LITERATURE

Although utilitarian, multi-UAV networks are mired with its own set of challenges that must be addressed. Of particular importance is the lack of available spectrum for UAV communications [5], [6]. Despite the allocation of parts of the L-band and C-band for UAV control and non-payload communications (CNPC) by the International Telecommunications Union (ITU) [5], spectrum scarcity is still a challenge. In particular, many other existing systems, e.g., aeronautical communication systems, are also operating on both the L-band and C-band [5]–[7]. In this aspect, a hybrid-duplex (HBD) UAV communication system (UCS), i.e., HBD-UCS, can be a direct solution address spectrum scarcity in UAV communications. The HBD paradigm enables UAVs with existing half-duplex (HD) communication systems, i.e., HD-UCS to simultaneously operate on the same spectrum with full-duplex (FD) ground stations (GSs), effectively doubling spectrum efficiency. However, the simultaneous transmission and reception of signals results in self-interference (SI) at the FD-enabled GS, which can be mitigated via passive or active SI mitigation architectures [8], [9]. The former entails introducing path loss and shadowing, e.g., through antenna placements, while the latter involves canceling SI in the analog or digital domain [9]. Even after SI mitigation, residual SI can still remain due to non-ideal FD transceiver impairments, such as carrier phase noise and imperfect

The associate editor coordinating the review of this manuscript and approving it for publication was Jiayi Zhang.

SI channel estimation, which limits the advantages of FD transmissions [9].[1]

Although one could argue that spectrum scarcity can be addressed via an FD-UCS, i.e., UAVs and GSs operating in FD mode, such a system may encounter challenges in meeting FD transceiver design requirements due to size, weight, and power restrictions imposed upon UAVs. As such, the HBD paradigm enables existing HD-UCS to be retained while improving spectrum utilization, with applications seen in aeronautical communication systems [8], [14], UCSs [7], [15], [16], and cellular systems [17], [18].

Other than SI at the FD-enabled GS, inter-UAV interference is also experienced at the HD UAVs, which can be handled through interference management strategies. In multi-user systems, such as the HBD-UCS, interference can be handled by exploiting the structure of interference [19], [20]. For instance, an interference ignorant (II) interference management strategy treats interference as noise and is optimal in weak interference scenarios [21], [22]. In strong interference scenarios, decoding the interfering signal before interference cancellation, i.e., successive interference cancellation, is an effective interference management strategy [19], [20]. In contrast, the joint detection (JD) strategy, which jointly decode both desired and interfering signals, is optimal in both moderate and strong interference scenarios albeit at the cost of high computational complexity [22]–[25].

Another challenge faced by multi-UAV networks is the combined effect of fading and shadowing in UAV communications [6], [26], especially in urban environments [27]. To begin modeling the UAV communication channel, it is noted that channel measurement campaigns for UAV-to-ground links in [28] showed a close match between the measurement data and the Rician fading model. For UAV-to-UAV links, i.e., inter-UAV channels, measurement campaigns in [29] have also demonstrated the Rician fading channel as a suitable model for inter-UAV links, with the authors in [30] similarly employing the Rician fading model for inter-UAV links to account for the availability of line-of-sight (LOS) links, scattering, and reflection from the environment. Nonetheless, despite several recent works on UAV channel modeling, e.g., [31]–[34], channel models that jointly account for fading and shadowing have not been investigated extensively. In particular, the Rician fading model may not be accurate in a suburban environment as it does not account for shadowing due to terrain or buildings [6], [26], [27]. In the empirical data of [28], where the characterization of UAV communication channels in hilly terrain was studied, Rician shadowed fading, i.e., line-of-sight (LOS) blockage, was observed. However, due to the limited dynamic range of the transceiver used during the measurement campaign, the authors in [28] omitted measurement data containing LOS shadowing.

To address the above limitation, the Rician shadowed fading model presented in [15] is a suitable choice for UAV channel modeling. Through the Rician shadowed fading model, Rician fading or Rayleigh fading UAV channels [16] can be modeled as special cases. It is worth noting that the Rician shadowed fading model is one of several shadowed fading, i.e., composite fading, models available in the literature. Such composite fading models combine shadowing, i.e., large-scale fading, with small-scale fading, e.g., $\kappa-\mu$ or Rician fading,[2] with fluctuations caused by shadowing modeled using Gaussian, lognormal, gamma, or inverse Gaussian distributions [27], [35].[3] For the Rician shadowed fading model, one can employ the $\kappa-\mu$ shadowed fading model, where the non-centered Chi-squared and Nakagami-m distributions are assumed for the multipath and LOS components, respectively [35]–[38]. In particular, the non-centered Chi-squared distribution accounts for both the LOS and non-LOS (NLOS) components encountered over the UAV channel, while the degree of LOS shadowing is modeled through the Nakagami-m distribution. Thus, using the Rician shadowed fading model, the severity of LOS shadowing and the ratio of the LOS-to-NLOS components can be accurately captured through the Nakagami-m shaping parameter and the Rician K factor, respectively. Furthermore, in contrast to the $\kappa-\mu$ shadowed fading model which considers LOS and NLOS shadowing for more than one multipath cluster, only one multipath cluster with LOS shadowing is considered for the Rician shadowed fading model. On top of the Rician shadowed fading model, it was shown by Paris [36] that the $\kappa-\mu$ shadowed fading model includes the one-sided Gaussian, Rayleigh, $\kappa-\mu$, and Rician fading models as special cases, obtainable through the substitution of appropriate shaping parameters. However, the relevant statistics from [35] and [36] are represented in the form of complicated functions, such as the confluent hypergeometric function [39] and the Gauss hypergeometric function [40], which may not yield tractable solutions. In this aspect, one can adopt the Rician shadowed fading model presented in [15]. In particular, the work in [15] presented power series expressions for statistics in the Rician shadowed fading model. While the closed-form expressions in [15] enables tractable mathematical analysis, the generality of the Rician shadowed fading model using the power series approach, i.e., to obtain the Rician fading model, remains an open

[1] In the current work, we mainly focus on carrier phase noise and imperfect SI channel estimation as major sources of FD transceiver impairments. Other types of hardware imperfections include the limited dynamic range of analog-to-digital converters, [10]–[12], transceiver nonlinearities [10], [12], [13], and I/Q mismatch [13]. An analysis that accounts for these imperfections are left as future extensions of this work.

[2] Small-scale fading occurs when the received signal power undergoes variations due to LOS or NLOS components, multipath clustering with circularly symmetric or elliptical scattering, and power imbalance between the in-phase and quadrature signal components [35]. Depending on the type of environment, different kinds of small-scale fading can occur. For instance, Rician fading is commonly encountered in UAV communications [5], [28], which can be modeled using the non-centered Chi-squared distribution.

[3] Shadowing occurs when a communication link is obstructed by buildings or terrain [6], [26], [27], [35], causing the total received signal power to fluctuate randomly [35]. The resultant fluctuations can be modeled using the Gaussian, lognormal, gamma, or inverse Gaussian distributions [27], [35].

research problem which will be investigated in the present work.

Although UAV communications in the presence of shadowing has been studied in the literature, e.g., [2], [41], [42], these works have not considered Rician shadowed fading or Rician fading and are only valid for interference-free scenarios. For interference management strategies, the II approach has already been investigated from the outage probability perspective for aeronautical communications over Rician fading channels [8], [14], and for UAV communications over Rician fading channels [16] and Rician shadowed fading channels [15]. In particular, the work in [15] presented new power series expressions for statistics associated with the Rician shadowed fading model. Thereafter, closed-form outage probability expressions for the II detector involving signal-to-interference-plus-noise ratio (SINR) of the form $\frac{Z_0}{1+Z_1}$, where Z_0 and Z_1 denote the desired and interfering signals, respectively, were derived for the Rician shadowed fading model through a power series approach. Thus, through the power series approach in [15], one can easily obtain closed-form outage probability expressions for the II detector over Rician shadowed fading channels. In contrast, one may have to resort to numerical methods to evaluate the outage probability of the II detector using the statistics presented in [43, eq. (3)], [35, eq. (12)], and [36, eq. (4)]. For the JD strategy, closed-form outage probability expressions are only available for Rician fading channels, e.g., [7]. Therefore, the outage probability analysis of UAV communications for JD over Rician shadowed fading channels through closed-form expressions remains an open problem.

To this end, we extend the Rician shadowed fading model in [15] to include the Rician fading model as a special case. It is worth mentioning that closed-form power series expressions for the Rician fading model are already available in [44, Table I and Table II]. However, we present alternative power series representations for the Rician fading model using the Rician shadowed fading model in the current paper. Therefore, we demonstrate that the Rician shadowed fading model in the present paper unifies Rician shadowed fading, Rician fading, and Rayleigh fading under the same power series-based model. Through the newly obtained closed-form expressions for the Rician shadowed fading model, we conduct an outage probability analysis of HBD UAV communications for multi-UAV networks in both Rician shadowed fading and Rician fading environments. Specifically, the outage probability analysis takes into consideration the effects of inter-UAV interference, SI, fading, and shadowing for the II and JD interference management approaches. Additionally, it is worth noting that the current paper is an extension of the work in [15], where the UAV-to-GS and the SI links are modeled as Rician fading channels. In contrast, the present work models the UAV channels and SI channel using the Rician shadowed fading model. As such, the system model and the subsequent analysis in [15] can be obtained in the present work as specific cases, thus illustrating the generality of the employed Rician shadowed fading model in the present paper.

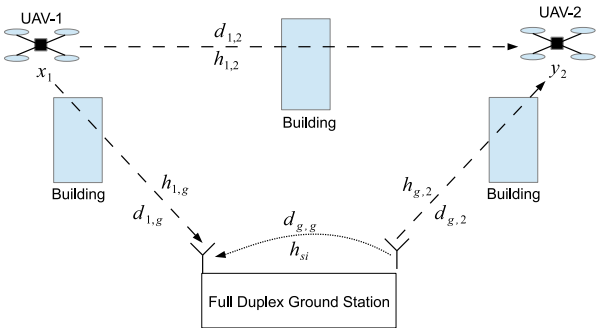

FIGURE 1. Unmanned Aerial Vehicle 1 (UAV-1) and Unmanned Aerial Vehicle 2 (UAV-2) operating in HD mode while communicating with the FD ground station (GS) over Rician shadowed fading channels.

Thus, the main contributions of this paper are summarized below.

B. MAIN CONTRIBUTIONS

- The present paper proposes a novel approach towards obtaining alternative power series representations of the probability density function (PDF), cumulative distribution function (CDF), and fractional moment for both the Rician fading and the Rician shadowed fading models.
- From the derived equations, closed-form outage probability expressions for the II and joint detectors using alternative power series expressions for the Rician shadowed fading and Rician fading models are obtained. To the best of our knowledge, the closed-form outage probability expressions and analysis are unavailable in the literature.
- Although counter-intuitive, it is shown that the impact of shadowing on the SI link at the FD-enabled GS is negligible. We also show that severe shadowing on the desired link with strong LOS component, as compared to weak LOS component, causes reduction in reliability even when SI mitigation measures are implemented.
- At UAV-2, the effect of severe shadowing on the desired link with strong LOS components is shown to be less severe for the joint detector than for the II detector.

The remainder of this paper is organized as follows. The system model is introduced in Section II, with alternative expressions for both Rician fading and Rician shadowed fading models presented in Section III. Outage probability expressions are presented in Section IV, with numerical results discussed in Section V before the conclusion of the paper in Section VI.

II. SYSTEM MODEL

The multi-UAV HBD-UCS operating in a suburban environment is shown in Fig. 1. In particular, it is assumed that the HD UAV-1 is simultaneously transmitting data to the FD-enabled GS while the HD UAV-2 is receiving control information on the same channel (Fig. 1). Such an arrangement enables the HBD-UCS to utilize spectrum efficiently, which is a challenge in UAV communications [5].

Another major issue in multi-UAV networks is the interference present in the HBD-UCS [45]. In Fig. 1, signals from Unmanned Aerial Vehicle 1 (UAV-1) are transmitted to both GS and Unmanned Aerial Vehicle 2 (UAV-2) as the signal-of-interest (SOI) and interference, respectively. Simultaneously at the FD-enabled GS, signals are transmitted to UAV-2. Consequently, inter-UAV interference and SI are experienced at UAV-2 and the FD-enabled GS, respectively.

In a suburban environment, it is likely for LOS components to be obstructed by buildings [6], [26], [27]. As such, Rician shadowed fading [35] is assumed on all UAV links ($h_{1,g}$, $h_{g,2}$, $h_{1,2}$) to adequately model the suburban UAV communication channels. As in [7], UAV mobility is assumed to be compensated in this paper. For SI channel modeling at the FD-enabled GS, recent literature have assumed the Rayleigh fading model [17], [18], [46] or the Rician fading model [10]. However, the present paper models the SI link (h_{si}) at the FD-enabled GS as a Rician shadowed fading channel. Such an assumption enables the analysis to consider the effects of passive SI suppression through shadowing experienced on the SI channel. Additionally, Rayleigh fading can be obtained through the Rician shadowed fading model as a special case by letting the Rician K factor be zero. Also, it is assumed that the SI signal undergoes active SI mitigation after passive SI suppression at the FD-enabled GS. Thus, only residual SI is considered at the GS.

A. GROUND STATION

At the GS, let the SOI transmitted from UAV-1 be $x_1[t]$, the signal transmitted from GS be $x_{gs}[t]$, and the SI be $x_{si}[t]$, where $x_{si}[t] = x_{gs}[t]$. Also, let $h_{1,g}[t]$, h_{si}, and $\widetilde{h}_{si} = h_{si} - \widehat{h}_{si}$ be the channel between UAV-1 and GS, the SI channel gain, and the SI channel gain estimate error, respectively, where $\widehat{h}_{si}$ is the imperfect estimation of the SI channel gain. Then, the received signal at GS can be written as [9]:

$$y_{gs}[t] = \sqrt{\Omega_X} h_{1,g}[t] x_1[t] + \sqrt{\Omega_X \alpha_{g,g}} |h_{si}| \gamma_\phi w_\phi[t] + \sqrt{\Omega_X \alpha_{g,g}} \cdot |\widetilde{h}_{si}| x_{si}[t] + w_g[t], \quad (1)$$

where $w_g[t]$ is the additive white Gaussian noise (AWGN) at GS with zero-mean and variance σ_g^2, and $w_\phi[t]$ is the Gaussian distributed phase noise term with zero-mean and unit variance, scaled by phase noise strength γ_ϕ [9].[4] The imperfect SI channel estimate ($\widetilde{h}_{si}$) is modeled as a circularly symmetric zero-mean complex Gaussian random variable (RV) with variance ϵ to model the worst case residual SI [47].

Using the free space path loss model, the average received signal power of the SOI (Ω_X), normalized by σ_g^2, is defined as:

$$\Omega_X \propto \frac{P_t}{(d_{1,g})^n \sigma_g^2}, \quad (2)$$

where P_t and $d_{1,g}$ are the transmit power (Watts) and distance (Km), respectively. It should be pointed out that $h_{1,g}[t]$ is chosen as the reference link in this work. Thus, the average received signal power in the other links are expressed relative to $h_{1,g}[t]$, using the multiplicative factor ($\alpha_{i,j}$) defined as:

$$\alpha_{i,j} = \left(\frac{d_{1,g}}{d_{i,j}}\right)^n, i \in \{g, 1\}, j \in \{g, 2\}, i \neq j. \quad (3)$$

For $i = j = g$, $\alpha_{g,g}$ is treated as a scaling variable for the average residual SI power at the GS. Together with $\alpha_{g,g}$, σ_g^2, and ϵ, the amount of SI suppression is quantified as $\frac{1}{\alpha_{g,g}\epsilon\sigma_g^2}$ [8], [47].

B. UNMANNED AERIAL VEHICLE 2

At UAV-2, let the SOI transmitted from GS be $x_{gs}[t]$, and the inter-UAV interference from UAV-1 be $x_1[t]$. Also, let $h_{g,2}[t]$ and $h_{1,2}[t]$ be the channels between GS and UAV-2, and UAV-1 and UAV-2, respectively. Then, the received signal at UAV-2 can be expressed as:

$$y_2[t] = \sqrt{\Omega_X \alpha_{g,2}} h_{g,2}[t] x_{gs}[t] + \sqrt{\Omega_X \alpha_{1,2}} h_{1,2}[t] x_1[t] + w_2[t], \quad (4)$$

where $w_2[t]$ is the AWGN at UAV-2 with zero-mean and variance σ_2^2. Additionally, $\Omega_X \alpha_{g,2}$ and $\Omega_X \alpha_{1,2}$ respectively indicate the average received signal powers of the SOI and interfering signal. Due to the presence of interference at both the FD-enabled GS and UAV-2, II and JD interference management approaches are considered in this work.

III. ALTERNATIVE EXPRESSIONS FOR THE RICIAN SHADOWED FADING MODEL

The $\kappa - \mu$ shadowed fading model has κ, μ and m as shaping parameters [35]. Specifically, κ represents the ratio between the total powers of the dominant component to the scattered component while μ denotes the number of multipath clusters. The variable m denotes the shadowing severity, obtained through the Nakagami-m distribution [35].

For a Rician shadowed fading channel h, the channel gain $|h|^2$ is obtained by setting $\mu = 1$ and letting κ be the Rician K factor [35], [36], i.e., $\kappa = K$, as follows [35, eq. (8)]:

$$|h|^2 = \left[X + \xi p\right]^2 + Y^2, \quad (5)$$

where $p = \sqrt{\frac{K}{1+K}}$, X and Y are mutually independent Gaussian RVs with

$$E\{X\} = E\{Y\} = 0, E\{X^2\} = E\{Y^2\} = \sigma^2, \quad (6)$$

and ξ is a Nakagami-m RV with $E\{\xi^2\} = 1$. The term $\left[X + \xi p\right]^2$ represents the dominant component and it contains both scattering and LOS components that are subjected to shadowing, while Y^2 represents the non-dominant component and it contains only the scattered component [30]. Additionally, under the obtained Rician shadowed fading model, LOS shadowing is modeled using ξ, with m indicating the severity of the shadowing [35]. From (5), the probability

[4] The scaling factor γ_ϕ models the jitter present in oscillators due to hardware imperfections [9]

density function (PDF) of $|h|^2$, i.e., Rician shadowed fading PDF, can be obtained from [35, Table I] as:

$$f_{|h|^2}(x) = \frac{m^m(1+K)}{\Omega(K+m)^m}\exp\left(\frac{-(1+K)x}{\Omega}\right) \times {}_1F_1\left(m;1;\frac{K(1+K)}{(K+m)\Omega}x\right), \quad (7)$$

where Ω and ${}_1F_1(\bullet)$ are the average received power and the confluent Hypergeometric function [39], respectively.

As the $\kappa-\mu$ shadowed fading model includes the Rician fading and the Rician shadowed fading models as specific cases, it is possible to obtain the Rician fading model from [35, Table I]. However, in its current form, important performance metrics, such as outage probability, are not easily obtainable from (7). Therefore, we present alternative closed-form expressions for the Rician shadowed fading and the Rician fading models in the subsequent sections based on the work in [15].

A. RICIAN SHADOWED FADING MODEL

Let $\overline{a}(n,\Omega,K,m,\gamma)$ be defined as:

$$\overline{a}(n,\Omega,K,m,\gamma) = \sum_{i=0}^{n}(-1)^{n-i}\left(\frac{m}{K+m}\right)^m\frac{(m)_i}{\Gamma^2(i+1)} \times\left(\frac{K}{K+m}\right)^i\left(\frac{1+K}{\Omega}\right)^{n+1}\frac{\gamma^{n+1}}{(n-i)!(n+1)}. \quad (8)$$

Then, alternative power series representations of the Rician shadowed fading PDF and the corresponding CDF are presented as follows.

Theorem 1: The PDF of $|h|^2$ can be represented as the following power series:

$$f_{|h|^2}(x) \approx \sum_{n=0}^{K_{tr}}\overline{a}(n,\Omega,K,m,1)(n+1)x^n, \quad (9)$$

where K_{tr} denotes the truncation order.

Proof: The proof can be found in [15] and is reproduced in Appendix A. ■

Theorem 2: The CDF of $|h|^2$ can be expressed as the following power series:

$$F_{|h|^2}(\gamma) = \int_0^{\gamma} f_{|h|^2}(x)dx \approx \sum_{n=0}^{K_{tr}}\overline{a}(n,\Omega,K,m,\gamma). \quad (10)$$

Proof: The CDF is obtained by interchanging the summation and integration, i.e., term-wise integration [39]. ■

Theorem 3: The l^{th} moment of $|h|^2$ is given as [35, eq. (10)]:

$$E\left\{\left(|h|^2\right)^l\right\} = \left(\frac{\Omega}{1+K}\right)^l\Gamma(1+l)\left(\frac{m}{K+m}\right)^{m-1-l} \times {}_2F_1\left(1-m,1+l;1;\frac{-K}{m}\right), \quad (11)$$

where ${}_2F_1(\bullet)$ is the Gauss hypergeometric function [40].

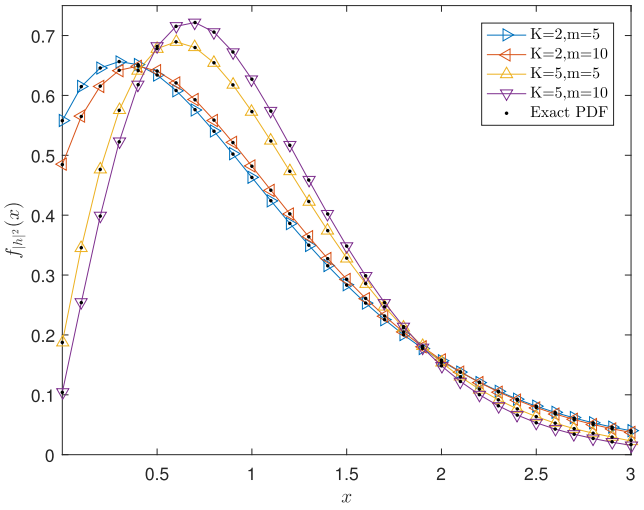

FIGURE 2. Comparison between the exact PDF of $|h|^2$ and power series approximation equivalent for $\Omega = 1$ and $K_{tr} = 50$.

Fig. 2 shows the power series representation of $f_{|h|^2}(x)$, computed from (9), with the exact PDF in (7) plotted for comparison. It can be seen that (9) provides a close fit to the exact PDF at the cost of computation time, which increases as $m \to \infty$. Additionally, although not plotted in Fig. 2, one obtains the Rician fading PDF by letting $m \to \infty$.

The closed-form expressions of the PDF, CDF and fractional moments of $|h|^2$, given in (9), (10), and (11), respectively, are useful in evaluating performance metrics, such as outage probability, in shadowing environments.

B. RICIAN FADING MODEL

To understand the impact of shadowing, (8) and (11) can be evaluated for large values of m. In particular, one obtains the Rician fading channel h' from the Rician shadowed fading channel h as $m \to \infty$. In the following Corollaries, new closed-form expressions for Rician fading models are presented.

Corollary 1: As $m \to \infty$, (8) can be expressed as:

$$\widehat{a}(n,\Omega,K,\gamma) = \sum_{i=0}^{n}\frac{(-1)^{n-i}K^i}{\Gamma^2(i+1)}\left(\frac{1+K}{\Omega}\right)^{n+1}\frac{\exp(-K)\gamma^{n+1}}{(n-i)!(n+1)}. \quad (12)$$

Proof: The proof can be found in Appendix B. ■

Remark 1: Although not shown in Corollary 1, it should be noted that $\widehat{a}(n,\Omega,K,\gamma)$ in (12) reduces as $K \to \infty$.

Corollary 2: The PDF $\left(f_{|h'|^2}(\bullet)\right)$ and CDF $\left(F_{|h'|^2}(\bullet)\right)$ of the Rician fading channel h' can be represented as the following power series:

$$f_{|h'|^2}(x) \approx \sum_{n=0}^{K_{tr}}\widehat{a}(n,\Omega,K,1)(n+1)x^n, \quad (13)$$

$$F_{|h'|^2}(\gamma) \approx \sum_{n=0}^{K_{tr}}\widehat{a}(n,\Omega,K,\gamma), \quad (14)$$

where $\widehat{a}(n,\Omega,K,\gamma)$ is given in (12).

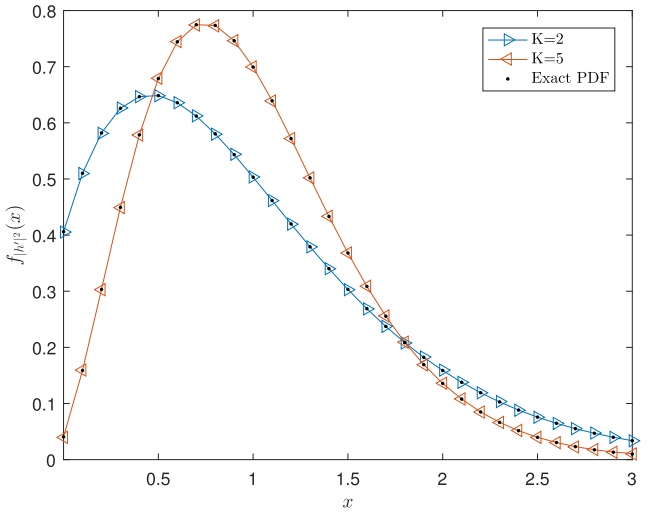

FIGURE 3. Comparison between the exact PDF of $|h'|^2$ and power series approximation equivalent for $\Omega = 1$ and $K_{tr} = 50$.

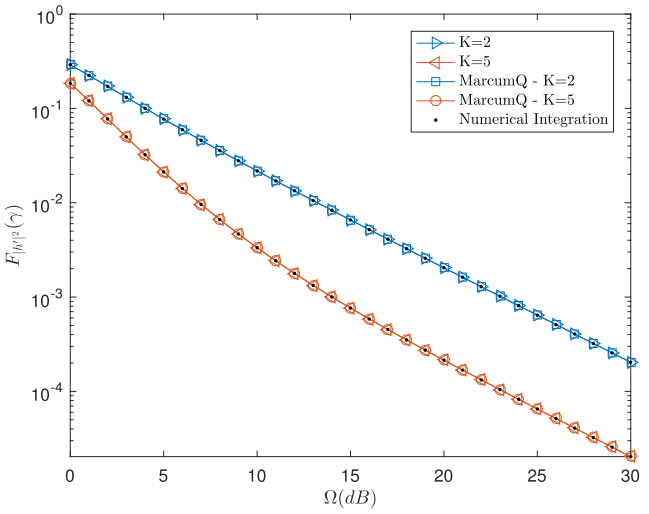

FIGURE 4. Comparison between the exact CDF of $|h'|^2$ and power series approximation equivalent for $\gamma = 0.5$ and $K_{tr} = 50$.

Proof: From (12), algebraic manipulation yields the power series expression of $f_{|h'|^2}(\bullet)$ and $F_{|h'|^2}(\bullet)$ in (13) and (14), respectively. ■

Corollary 3: The closed-form expression for the l^{th} moment of $|h'|^2$ is:

$$E\left\{\left(|h'|^2\right)^l\right\} = \lim_{m\to\infty} E\left\{\left(|h|^2\right)^l\right\} \approx \left(\frac{\Omega}{1+K}\right)^l \Gamma(1+l) \sum_{n=0}^{K_{tr}} \frac{(-l)_n}{n!(1)_n}(-K)^n. \quad (15)$$

Proof: The proof can be found in Appendix C. ■

The Rician PDF in (13) is plotted in Fig. 3 and compared against the exact Rician fading PDF

$$f_{|h'|^2}(x) = \frac{K+1}{\Omega} \exp\left(-K - \frac{K+1}{\Omega}x\right) I_0\left(2\sqrt{\frac{K(K+1)}{\Omega}x}\right),$$

where $I_0(\cdot)$ is the modified Bessel function of the first kind with zero order [39]. It can be observed that (13) provides a close fit to the exact PDF in Fig. 3.

The Rician fading CDF $F_{|h'|^2}(\gamma)$ in (14) is plotted in Fig. 4. When compared against the numerical integration of $f_{|h'|^2}(x)$ and the exact CDF, $F_{|h'|^2}(\gamma) = 1 - Q_1\left(\sqrt{2K}, \sqrt{\frac{2(K+1)\gamma}{\Omega}}\right)$ where $Q_1(\cdot,\cdot)$ is the Marcum Q function [44], a close fit is also observed. Similar observations are also made in Fig. 5 when (15) is compared against $E\left\{\left(|h'|^2\right)^l\right\} = \Gamma(1+l)\left[\frac{\Omega}{1+K}\right]^l {}_1F_1(-l, 1; -K)$ [44, Table II].

Evidently, (8) and (11) become independent of m as $m \to \infty$. More importantly, Corollaries 1 and 3 show that the computed values of (8) and (11) decreases and increases, respectively, based on the Rician K factor as $m \to \infty$. The presented power series representations of the Rician shadowed fading and Rician fading models in this section

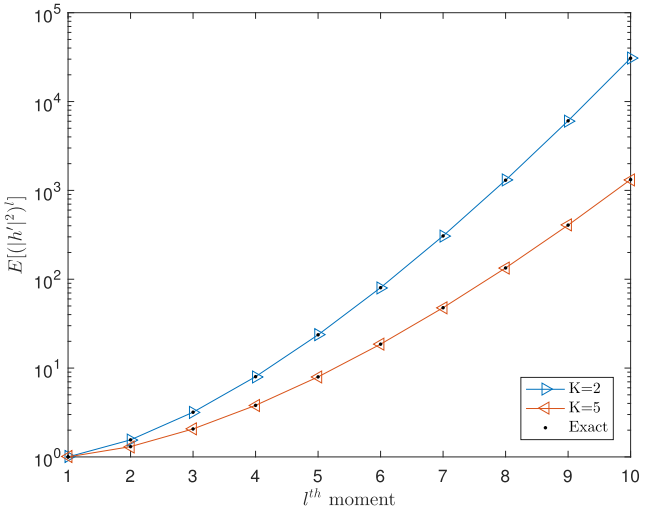

FIGURE 5. Comparison between the exact fractional moment of $|h'|^2$ and power series approximation equivalent for $\Omega = 1$ and $K_{tr} = 50$.

are summarized in Table 1.[5] Together, these observations and expressions are essential in evaluating the outage probability of the HBD-UCS, which is discussed in Section IV.

IV. OUTAGE PROBABILITY DERIVATIONS

In this section, closed-form outage probability expressions are derived for the HBD-UCS. The transmission rates of UAV-1 and GS are defined as R_1^{HBD} and R_{gs}^{HBD}, respectively, with HBD system sum rate defined as $R_{sum}^{HBD} = R_1^{HBD} + R_{gs}^{HBD}$. Similarly for HD transmission, the transmission rates of UAV-1 and GS are defined as R_1^{HD} and R_{gs}^{HD},

[5]The functions $\gamma(\cdot,\cdot)$, $I_0(\cdot)$, $Q_1(\cdot,\cdot)$, and ${}_1F_1(\bullet)$ represent the lowercase incomplete gamma function [35], the modified Bessel function of the first kind with zero order [39], the Marcum Q function [44], and the confluent Hypergeometric function [39], respectively. The fractional moment of $|h|^2$, i.e., $E\{(|h|^2)^j\}$ is given in (11) while $\bar{a}(n, \Omega, K, m, 1)$ and $\hat{a}(n, \Omega, K, \gamma)$ are given in (8) and (12), respectively.

TABLE 1. Summary of presented closed-form expressions for the Rician shadowed fading and Rician fading models.

Fading Model	Power Series Representation (Current Work)	State-of-the-Art	Reference
Rician shadowed	$f_{\lvert h\rvert^2}(x) \approx \sum_{n=0}^{K_{tr}} \overline{a}(n,\Omega,K,m,1)(n+1)x^n$	$f_{\lvert h\rvert^2}(x) = \frac{m^m(1+K)}{\Omega(K+m)^m}\exp\left(\frac{-(1+K)x}{\Omega}\right){}_1F_1\left(m;1;\frac{K(1+K)x}{(K+m)\Omega}\right)$	[35]
		$f_{\lvert h\rvert^2}(x) = \sum_{n=0}^{\infty}\sum_{i=0}^{n}\sum_{j=0}^{n}\frac{(-1)^{i+j}}{\Gamma[i+1]j!}\binom{n}{i}\binom{n}{n-j}E\{(\lvert h\rvert^2)^j\}x^i\exp(-x)$	[35]
Rician shadowed	$F_{\lvert h\rvert^2}(\gamma) \approx \sum_{n=0}^{K_{tr}} \overline{a}(n,\Omega,K,m,\gamma)$	$F_{\lvert h\rvert^2}(x) = \sum_{n=0}^{\infty}\sum_{i=0}^{n}\sum_{j=0}^{n}\frac{(-1)^{i+j}}{\Gamma(i+2)j!}\binom{n}{i}\binom{n}{n-j}E\{(\lvert h\rvert^2)^j\}x^{i+1}+\gamma(1,x)$	[35]
Rician	$f_{\lvert h'\rvert^2}(x) \approx \sum_{n=0}^{K_{tr}} \widehat{a}(n,\Omega,K,1)(n+1)x^n$	$f_{\lvert h'\rvert^2}(x) = \frac{K+1}{\Omega}\exp\left(-K-\frac{K+1}{\Omega}x\right)I_0\left(2\sqrt{\frac{K(K+1)}{\Omega}x}\right)$	[44]
Rician	$F_{\lvert h'\rvert^2}(\gamma) \approx \sum_{n=0}^{K_{tr}} \widehat{a}(n,\Omega,K,\gamma)$	$F_{\lvert h'\rvert^2}(\gamma) = 1-Q_1\left(\sqrt{2K},\sqrt{\frac{2(K+1)\gamma}{\Omega}}\right)$	[44]
Rician	$E\{(\lvert h'\rvert^2)^l\} \approx \left(\frac{\Omega}{1+K}\right)^l\Gamma(1+l)\sum_{n=0}^{K_{tr}}\frac{(-l)_n}{n!(1)_n}(-K)^n$	$E\{(\lvert h'\rvert^2)^l\} = \Gamma(1+l)\left[\frac{\Omega}{1+K}\right]^l{}_1F_1(-l,1;-K)$	[44]

respectively, with HD system sum rate $R_{sum}^{HD} = R_1^{HD} + R_{gs}^{HD}$. To maintain a fair comparison between HBD and HD systems, we let $R_i^{HBD} = \frac{1}{2}R_i^{HD}$ for $i \in \{1, gs\}$ [48]. Based on these definitions, the HBD and HD outage probabilities at GS and UAV-2 are defined in the following subsections.

A. HYBRID-DUPLEX OUTAGE PROBABILITY

Starting with the FD-enabled GS, strong SI is experienced due to the simultaneous transmission and reception of $x_{gs}[t]$ and $x_1[t]$, respectively. Let the instantaneous received signal power of the SOI at GS be $X_1 = \Omega_X|h_{1,g}|^2$, modeled as a Rician shadowed distributed RV with Rician K factor K_{X_1} and shadowing severity parameter m_{X_1}. Also, Let the instantaneous received signal power of the SI components be $Y_{si,1} = \Omega_X\alpha_{g,g}\gamma_\phi^2|h_{si}|^2$ and $Y_{si,2} = \Omega_X\alpha_{g,g}\epsilon|\widetilde{h}_{si}|^2$. The RVs, $Y_{si,1}$ and $Y_{si,2}$, are modeled as a Rician shadowed distributed RV with Rician K factor $K_{Y_{si,1}}$ and shadowing parameter $m_{Y_{si,1}}$, and an exponentially distributed RV, respectively.

At UAV-2, let the instantaneous received signal power of the SOI and interference be $X_{gs} = \Omega_X\alpha_{g,2}|h_{g,2}|^2$ and $Y_1 = \Omega_X\alpha_{1,2}|h_{1,2}|^2$, respectively. Both X_{gs} and Y_1 are respectively modeled as independent Rician shadowed distributed RVs, with Rician K factors $K_{X_{gs}}$ and K_{Y_1}, and shadowing severity parameters $m_{X_{gs}}$ and m_{Y_1}.

1) GROUND STATION

At the FD-enabled GS, SI mitigation is imperfect due to phase noise and SI channel estimation error. As a result, residual SI is experienced at the GS. Thus, an II detector is assumed at the GS, which treats residual SI ($Y_{si,1}$, $Y_{si,2}$) as noise when detecting the SOI (X_1). Let the outage event, outage probability, and the HBD threshold at the FD-enabled GS be

$$\mathcal{O}_{gs}^{HBD} = \left\{h_{1,g}, h_{si}, \widetilde{h}_{si} : R_1^{HBD} \geq \log_2\left(1+\frac{X_1}{Y_{si,1}+Y_{si,2}+1}\right)\right\}, Pr\left(\mathcal{O}_{gs}^{HBD}\right),$$

and $\gamma_{th,gs}^{HBD} = 2^{R_1^{HBD}} - 1$, respectively.

Theorem 4: The closed-form outage probability at GS over Rician shadowed fading channels is:

$$Pr\left(\mathcal{O}_{gs}^{HBD}\right) \approx \sum_{n=0}^{K_{tr}}\sum_{l_1+l_2+l_3=n+1}\overline{a}\left(n,\Omega_X,K_{X_1},m_{X_1},\gamma_{th,gs}^{HBD}\right) \times\frac{(n+1)!}{l_1!\cdot l_2!\cdot l_3!}E\{Y_{si,1}^{l_1}\}E\{Y_{si,2}^{l_2}\}, \tag{16}$$

where

$$E\{Y_{si,1}^{l_1}\} = \Gamma(1+l_1) \times\left(\frac{\alpha_{g,g}\gamma_\phi^2}{1+K_{Y_{si,1}}}\right)^{l_1}\left(\frac{m_{Y_{si,1}}}{K_{Y_{si,1}}+m_{Y_{si,1}}}\right)^{m_{Y_{si,1}}-1-l_1} \times{}_2F_1\left(1-m_{Y_{si,1}},1+l_1;1;\frac{-K_{Y_{si,1}}}{m_{Y_{si,1}}}\right)(\Omega_X)^{l_1}, \tag{17}$$

$$E\{Y_{si,2}^{l_2}\} = \Gamma(1+l_2)(\alpha_{g,g}\epsilon)^{l_2}(\Omega_X)^{l_2}. \tag{18}$$

Proof: The outage probability at GS can be obtained as $Pr\left(\mathcal{O}_{gs}^{HBD}\right) = E\left\{F_{X_1}\left(\gamma_{th,gs}^{HBD}(1+Y_{si,1}+Y_{si,2})\right)\right\}$, where $F_{X_1}(\bullet)$ is the CDF of X_1 obtained from (10). The final expression for $Pr\left(\mathcal{O}_{gs}^{HBD}\right)$ can be calculated from [44, eq. (8)], with the proof of convergence given in Appendix D. ■

As shadowing is considered at the GS, the impact of shadowing on the SI link due to passive SI suppression can be investigated using (16). Furthermore, for the case of Rician fading channels, we present an alternative outage probability expression from (16) in the following Corollary.

Corollary 4: The closed-form outage probability at GS over Rician fading channels is:

$$Pr\left(\mathcal{O}_{gs}^{HBD*}\right) \approx \sum_{n=0}^{K_{tr}}\sum_{l_1+l_2+l_3=n+1}\widehat{a}\left(n,\Omega_X,K_{X_1},\gamma_{th,gs}^{HBD}\right) \times\frac{(n+1)!}{l_1!\cdot l_2!\cdot l_3!}E\{Y_{si,1}^{l_1*}\}E\{Y_{si,2}^{l_2}\}, \tag{19}$$

where $Y_{si,1}^{l_1*}$ is a RV defined using the Rician fading model and

$$E\{Y_{si,1}^{l_1*}\} = \Gamma(1+l_1)\left(\frac{\alpha_{g,g}\gamma_\phi^2\Omega_X}{1+K_{Y_{si,1}}}\right)^{l_1}\sum_{i=0}^{K_{tr}}\frac{(-l_1)_i}{i!(1)_i}(-K_{Y_{si,1}})^i. \tag{20}$$

Proof: Replacing $\overline{a}\left(n, \Omega_X, K_{X_1}, m_{X_1}, \gamma_{th,gs}^{HBD}\right)$ in (16) with (12) and applying (15) to evaluate $E\{Y_{si,1}^{l_1*}\}$ yields (19). Additionally, it can be shown that (19) converges absolutely by following the same steps in Appendix D. ■

The closed-form expression in Corollary 4 are used as a benchmark to evaluate the reliability of the GS over Rician fading channels. From [8], it is known that the FD-enabled GS becomes interference-limited at high SNR regimes. Thus, in the following Corollary, the asymptotic outage probability of the FD-enabled GS over Rician shadowed fading channels and Rician fading channels is presented.

Corollary 5: The closed-form asymptotic outage probability expressions at the GS over Rician shadowed fading channels $\left(Pr\left(\mathcal{O}_{gs,\infty}^{HBD}\right)\right)$ and Rician fading channels $\left(Pr\left(\mathcal{O}_{gs,\infty}^{HBD*}\right)\right)$ are:

$$Pr\left(\mathcal{O}_{gs,\infty}^{HBD}\right) \approx \sum_{n=0}^{K_{tr}} \sum_{l_1+l_2=n+1} \overline{a}\left(n, 1, K_{X_1}, m_{X_1}, \gamma_{th,gs}^{HBD}\right) \times \frac{(n+1)!}{l_1! \cdot l_2!} M\{Y_{si,1}^{l_1}\} M\{Y_{si,2}^{l_2}\}, \tag{21}$$

$$Pr\left(\mathcal{O}_{gs,\infty}^{HBD*}\right) \approx \sum_{n=0}^{K_{tr}} \sum_{l_1+l_2=n+1} \widehat{a}\left(n, 1, K_{X_1}, \gamma_{th,gs}^{HBD}\right) \times \frac{(n+1)!}{l_1! \cdot l_2!} M\{Y_{si,1}^{l_1*}\} M\{Y_{si,2}^{l_2}\}, \tag{22}$$

where $M\{Z^l\} = E\{Z^l\}/(\Omega_X)^l$ is the normalized l^{th} moment of RV Z [8].

Proof: The proof is given in Appendix E. ■

As the FD-enabled GS is interference-limited [8], Corollary 5 can be used to obtain the outage probability error floor, which is useful in determining how SI and shadowing affects reliability. Further discussion on the outage probability at GS are presented in Section V.

2) UNMANNED AERIAL VEHICLE 2 (INTERFERENCE IGNORANT DETECTOR)

At UAV-2, inter-UAV interference (Y_1) is treated as noise when the II detector is detecting the SOI (X_{gs}). Let the outage event, outage probability, and the HBD threshold at UAV-2 be

$$\mathcal{O}_2^{HBD(II)} = \left\{h_{g,2}, h_{1,2} : R_{gs}^{HBD} \geq \log_2\left(1 + \frac{X_{gs}}{Y_1+1}\right)\right\}, Pr\left(\mathcal{O}_2^{HBD(II)}\right),$$

and $\gamma_{th,2}^{HBD} = 2^{R_{gs}^{HBD}} - 1$, respectively.

Theorem 5: The closed-form outage probability expression with II detector at UAV-2 over Rician shadowed fading channels is:

$$Pr\left(\mathcal{O}_2^{HBD(II)}\right) \approx \sum_{n=0}^{K_{tr}} \sum_{j=0}^{n+1} \overline{a}\left(n, \Omega_X \alpha_{g,2}, K_{X_{gs}}, m_{X_{gs}}, \gamma_{th,2}^{HBD}\right) \times \binom{n+1}{j} E\{Y_1^j\}, \tag{23}$$

where

$$E\{Y_1^j\} = \left(\frac{\Omega_X \alpha_{1,2}}{1+K_{Y_1}}\right)^j \Gamma(1+j) \times \left(\frac{m_{Y_1}}{K_{Y_1}+m_{Y_1}}\right)^{m_{Y_1}-1-j} {}_2F_1\left(1-m_{Y_1}, 1+j; 1; \frac{-K_{Y_1}}{m_{Y_1}}\right).$$

Proof: The closed-form outage probability expression at UAV-2 can be obtained as

$$Pr\left(\mathcal{O}_2^{HBD(II)}\right) = E\left\{F_{X_{gs}}\left(\gamma_{th,2}^{HBD}(1+Y_1)\right)\right\},$$

where $F_{X_{gs}}(\bullet)$ is the CDF of X_{gs} from (10). The final expression for $Pr\left(\mathcal{O}_2^{HBD(II)}\right)$ is calculated from [44, eq. (8)]. Separately, it can be shown that (23) converges absolutely by repeating the same approach in Appendix D. ■

For the case of Rician fading channels, an alternative outage probability expression from (23) is presented in the following Corollary.

Corollary 6: The closed-form outage probability expression with II detector at UAV-2 over Rician fading channels is:

$$Pr\left(\mathcal{O}_2^{HBD(II)*}\right) \approx \sum_{n=0}^{K_{tr}} \sum_{j=0}^{n+1} \widehat{a}\left(n, \Omega_X \alpha_{g,2}, K_{X_{gs}}, \gamma_{th,2}^{HBD}\right) \times \binom{n+1}{j} E\{Y_1^{j*}\}, \tag{24}$$

where Y_1^{j*} is a RV defined using the Rician fading model and

$$E\{Y_1^{j*}\} = \left(\frac{\Omega_X \alpha_{1,2}}{1+K_{Y_1}}\right)^j \Gamma(1+j) \sum_{i=0}^{K_{tr}} \frac{(-j)_i}{i!(1)_i} (-K_{Y_1})^i.$$

Proof: Substituting $\overline{a}\left(n, \Omega_X \alpha_{g,2}, K_{X_{gs}}, m_{X_{gs}}, \gamma_{th,2}^{HBD}\right)$ in (23) with (12) yields (24). Similarly, applying (15) yields the closed-form expression for $E\{Y_1^{j*}\}$. Similar to (23), (24) is shown to be absolutely convergent by repeating the same approach in Appendix D. ■

As the II detector is interference-limited at high SNR regimes [8], characterizing the asymptotic outage probability will provide useful insights into how inter-UAV interference affects the error floor. In the following Corollary, the asymptotic outage probability of the II detector over Rician shadowed fading channels and Rician fading channels is presented.

Corollary 7: The closed-form asymptotic outage probability expressions for the II detector over Rician shadowed fading channels $\left(Pr\left(\mathcal{O}_{2,\infty}^{HBD(II)}\right)\right)$ and Rician fading channels $\left(Pr\left(\mathcal{O}_{2,\infty}^{HBD(II)*}\right)\right)$ are:

$$Pr\left(\mathcal{O}_{2,\infty}^{HBD(II)}\right) \approx \sum_{n=0}^{K_{tr}} \overline{a}\left(n, \alpha_{g,2}, K_{X_{gs}}, m_{X_{gs}}, \gamma_{th,2}^{HBD}\right) \times M\{Y_1^{n+1}\}, \tag{25}$$

$$Pr\left(\mathcal{O}_{2,\infty}^{HBD(II)*}\right) \approx \sum_{n=0}^{K_{tr}} \widehat{a}\left(n, \alpha_{g,2}, K_{X_{gs}}, \gamma_{th,2}^{HBD}\right) \times M\{Y_1^{n+1*}\}. \tag{26}$$

Proof: Corollary 7 is obtained using the same steps provided in Appendix E. ∎

With shadowing experienced on both the SOI link ($h_{g,2}$) and the interfering link ($h_{1,2}$), the impact of shadowing on the II detector can be investigated from (23). In addition, the II detector works well in weak interference scenarios [8]. Thus, it is of practical significance to understand the impact of inter-UAV interference and shadowing on outage probability, which is presented in Section V.

3) UNMANNED AERIAL VEHICLE 2 (JOINT DETECTOR)

The joint detector jointly estimates both the SOI (X_{gs}) and the inter-UAV interference signal (Y_1), with GS and UAV-1 transmitting under a sum rate constraint. In particular, the joint detector treats the GS signal X_{gs} as the SOI and the UAV-1 signal Y_1 as interference. As such, the joint detector decodes the SOI with the knowledge of interfering signal's structure. Such an arrangement enables UAV-1 to transmit at a higher rate than the capacity of the interfering link [49], with similar decoding algorithms investigated for interference-limited receivers in two-user interference channels [50], [51].

The outage event for the joint detector $\mathcal{O}_2^{HBD(JD)}$ can be defined as [7]:

$$\mathcal{O}_2^{HBD(JD)} = \mathcal{O}_{JD}^1 \cup \mathcal{O}_{JD}^2, \tag{27}$$

where

$$\mathcal{O}_{JD}^1 = \left\{ h_{g,2}, h_{1,2} : R_{gs}^{HBD} > \log_2\left(1 + X_{gs}\right) \right\}, \tag{28}$$

$$\mathcal{O}_{JD}^2 = \left\{ h_{g,2}, h_{1,2} : R_1^{HBD} + R_{gs}^{HBD} > \log_2\left(1 + X_{gs} + Y_1\right), \log_2\left(1 + \frac{X_{gs}}{1 + Y_1}\right) \le R_{gs}^{HBD} \le \log_2\left(1 + X_{gs}\right) \right\}. \tag{29}$$

The outage event $\left(\mathcal{O}_2^{HBD(JD)}\right)$ occurs if SOI detection fails $\left(\mathcal{O}_{JD}^1\right)$ or if the sum rate constraint is not met $\left(\mathcal{O}_{JD}^2\right)$.

Theorem 6: The closed-form expression for the outage probability with the joint detector at UAV-2 over Rician shadowed fading channels is:

$$\begin{aligned} Pr\left(\mathcal{O}_2^{HBD(JD)}\right) &\approx \sum_{n=0}^{K_{tr}} \bar{a}\left(n, \Omega_X \alpha_{g,2}, K_{X_{gs}}, m_{X_{gs}}, \gamma_{th,2}^{HBD}\right) \\ &+ \sum_{n=0}^{K_{tr}} \sum_{q=0}^{n} \sum_{k=0}^{q+1} \bar{a}\left(q, \Omega_X \alpha_{1,2}, K_{Y_1}, m_{Y_1}, 1\right) \\ &\times \bar{a}\left(n-q, \Omega_X \alpha_{g,2}, K_{X_{gs}}, m_{X_{gs}}, 1\right)(n+1)\binom{q+1}{k}(-1)^{q+1} \\ &\times G_1\left(q, k, b_2, \gamma_{th,2}^{HBD}\right) \frac{G_2\left(k+n-q+1, b_1, \gamma_{th,2}^{HBD}\right)}{k+n-q+1}, \end{aligned} \tag{30}$$

where

$$\begin{aligned} b_1 &= 2^{R_1^{HBD}}\left(2^{R_{gs}^{HBD}} - 1\right), b_2 = 2^{R_1^{HBD} + R_{gs}^{HBD}} - 1, \\ G_1\left(q, k, b_2, \gamma_{th,2}^{HBD}\right) &= (-b_2)^{q+1-k} - (-\gamma_{th,2}^{HBD})^{-k}, \\ G_2\left(k+n-q+1, b_1, \gamma_{th,2}^{HBD}\right) &= (b_1)^{k+n-q+1} \\ &- (\gamma_{th,2}^{HBD})^{k+n-q+1}. \end{aligned}$$

Proof: The proof pertaining to the derivation of the outage probability expression and it's convergence can be found in Appendix F. ∎

For the case of Rician fading, an alternative outage probability expression using (30) is presented in the following Corollary.

Corollary 8: The closed-form outage probability expression with the joint detector at UAV-2 over Rician fading channels is:

$$\begin{aligned} Pr\left(\mathcal{O}_2^{HBD(JD)*}\right) &\approx \sum_{n=0}^{K_{tr}} \widehat{a}\left(n, \Omega_X \alpha_{g,2}, K_{X_{gs}}, \gamma_{th,2}^{HBD}\right) \\ &+ \sum_{n=0}^{K_{tr}} \sum_{q=0}^{n} \sum_{k=0}^{q+1} \widehat{a}\left(q, \Omega_X \alpha_{1,2}, K_{Y_1}, 1\right) \\ &\times \widehat{a}\left(n-q, \Omega_X \alpha_{g,2}, K_{X_{gs}}, 1\right)(n+1)\binom{q+1}{k}(-1)^{q+1} \\ &\times G_1\left(q, k, b_2, \gamma_{th,2}^{HBD}\right) \frac{G_2\left(k+n-q, b_1, \gamma_{th,2}^{HBD}\right)}{k+n-q+1}. \end{aligned} \tag{31}$$

Proof: Equation (31) is obtained using the same approach in Corollary 6. Furthermore, it can be demonstrated that (31) converges absolutely by adopting the same technique used in Appendix F. ∎

At high SNR regimes, the joint detector has been shown to exhibit interference-free performance [7]. As it will be demonstrated in the next Corollary, the joint detector achieves zero outage probability at asymptotic SNR regimes over Rician shadowed fading channels and Rician fading channels.

Corollary 9: The joint detector attains zero outage probability over Rician shadowed fading channels and Rician fading channels at asymptotic SNR regimes.

Proof: The proof is provided in Appendix G. ∎

The joint detector works well when the SOI and the interfering signal are sufficiently strong [22], with Corollary 1 suggesting that a lower $Pr\left(\mathcal{O}_2^{HBD(JD)}\right)$ is attained when $K_{X_{gs}}$, K_{Y_1}, $m_{X_{gs}}$, and m_{Y_1} are high. To this end, the combined impact of inter-UAV interference and shadowing on the joint detector can be analyzed from (30), which is discussed in detail in Section V.

B. HALF-DUPLEX OUTAGE PROBABILITY

When operating in HD mode, interference is non-existent at both GS and UAV-2. Let the HD threshold at GS and UAV-2 be $\gamma_{th,gs}^{HD} = 2^{2R_1^{HBD}} - 1$ and $\gamma_{th,2}^{HD} = 2^{2R_{gs}^{HBD}} - 1$, respectively. Then, the HD outage probability at GS $\left(Pr\left(\mathcal{O}_{gs}^{HD}\right)\right)$ and

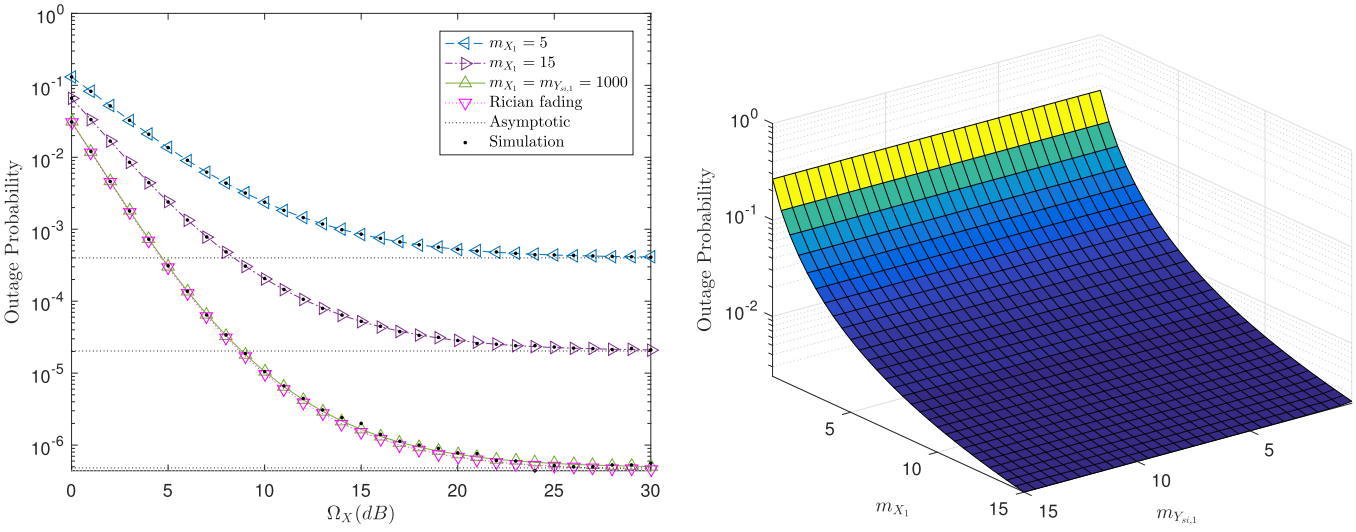

FIGURE 6. Outage probability at GS for $\alpha_{g,g} = 1$, $\epsilon = 0.01$, $\gamma_\phi^2 = -130$dBm, and $K_{X_1} = K_{Y_{si,1}} = 15$. (a) Impact of shadowing at GS for $m_{Y_{si,1}} = 10$. (b) Impact of shadowing at GS for $\Omega_X = 5dB$ and $0.5 \leq m_{X_1}, m_{Y_{si,1}} \leq 15$.

UAV-2 $\left(Pr\left(\mathcal{O}_2^{HD}\right)\right)$ over Rician shadowed fading channels is obtained from (10) as:

$$Pr\left(\mathcal{O}_{gs}^{HD}\right) \approx \sum_{n=0}^{K_{tr}} \overline{a}\left(n, \Omega_X, K_{X_1}, m_{X_1}, \gamma_{th,gs}^{HD}\right). \tag{32}$$

$$Pr\left(\mathcal{O}_{2}^{HD}\right) \approx \sum_{n=0}^{K_{tr}} \overline{a}\left(n, \Omega_X \alpha_{g,2}, K_{X_{gs}}, m_{X_{gs}}, \gamma_{th,2}^{HD}\right). \tag{33}$$

Adopting the same technique to derive Corollary 6 yields the following closed-form outage probability expressions over Rician fading channels:

$$Pr\left(\mathcal{O}_{gs}^{HD*}\right) \approx \sum_{n=0}^{K_{tr}} \widehat{a}\left(n, \Omega_X, K_{X_1}, \gamma_{th,gs}^{HD}\right). \tag{34}$$

$$Pr\left(\mathcal{O}_{2}^{HD*}\right) \approx \sum_{n=0}^{K_{tr}} \widehat{a}\left(n, \Omega_X \alpha_{g,2}, K_{X_{gs}}, \gamma_{th,2}^{HD}\right). \tag{35}$$

Finally, it should be noted that by repeating the steps in Appendix F, it can be shown that the HD outage probability expressions converge absolutely. Separately, operating the GS and UAV-2 in HD mode results in interference-free transmissions. As such, by utilizing the same approach in Appendix G, it can be shown that both the GS and UAV-2 achieves zero outage probability over Rician shadowed fading channels and Rician fading channels at asymptotic SNR regimes.

The HD outage probability expressions provide benchmark comparison against the HBD mode of operation at GS and UAV-2, which is discussed in Section V.

V. NUMERICAL RESULTS

Numerical results pertaining to the outage probability at UAV-2 and at the GS are presented in this section, along with Monte Carlo simulations conducted with 10^7 samples. The Monte Carlo simulations are conducted on MATLAB, using the *random* and *rand* functions. To maintain a fair comparison between the HBD-UCS and HD-UCS, we let $R_{sum}^{HD} = R_{sum}^{HBD} = 1$, with $\sigma_g^2 = \sigma_2^2 = -115dBm$.

TABLE 2. Error margin of the outage probability at GS.

	Ω_X = 5 dB	Ω_X = 15 dB	Ω_X = 30 dB
$m_{X_1} = 5$	4.68×10^{-5}	2.74×10^{-5}	1.14×10^{-5}
$m_{X_1} = 15$	1.34×10^{-6}	8.59×10^{-6}	8.51×10^{-6}
$m_{X_1} = m_{Y_{si,1}} = 1000$	1.98×10^{-6}	-	-
Rician fading	1.25×10^{-5}	-	-

A. IMPACT OF SHADOWING AT GS

Result 1: Shadowing on the SI link has negligible impact on outage probability at the GS.

The HBD outage probability at GS $\left(Pr\left(\mathcal{O}_{gs}^{HBD}\right)\right)$, given in (16), is shown in Fig. 6 for $m_{X_1} \in \{5, 15, 1000\}$. For the case of Rician fading channels, $Pr\left(\mathcal{O}_{gs}^{HBD}\right)$ is plotted using (19) which matches with (16) for $m_{X_1} = m_{Y_{si,1}} = 1000$. Likewise, $Pr\left(\mathcal{O}_{gs}^{HBD}\right)$ is plotted using (34) for the case of Rician fading channels. The error margins of the outage probability at GS are shown in Table 2.

From Fig. 6a, it can be seen that the outage probability drops more steeply as m_{X_1} increases due to less shadowing on the desired link ($h_{1,g}$) than the SI link (h_{si}). In Fig. 6b, it is observed that shadowing on the SI link ($m_{Y_{si,1}}$) has negligible impact on the outage probability, especially when $m_{Y_{si,1}}$ is large. From Corollary 3, it is shown that the fractional moment of a Rician shadowed RV is independent of m as $m \to \infty$. Therefore, the outage probability at the GS is independent of $m_{Y_{si,1}}$ as $m_{Y_{si,1}} \to \infty$. The trend in Fig. 6b

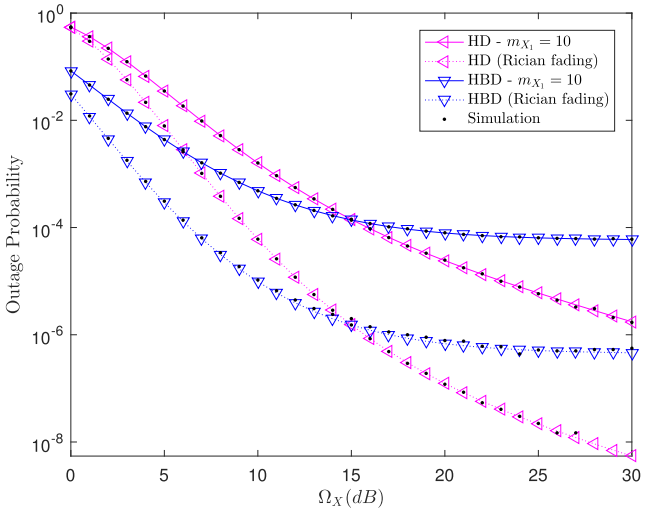

FIGURE 7. Outage probability at GS (HBD vs HD) for $\alpha_{g,g} = 1$, $\epsilon = 0.01$, $\gamma_\phi^2 = -130$dBm, $K_{X_1} = K_{Y_{si,1}} = 15$, $m_{Y_{si,1}} = 10$.

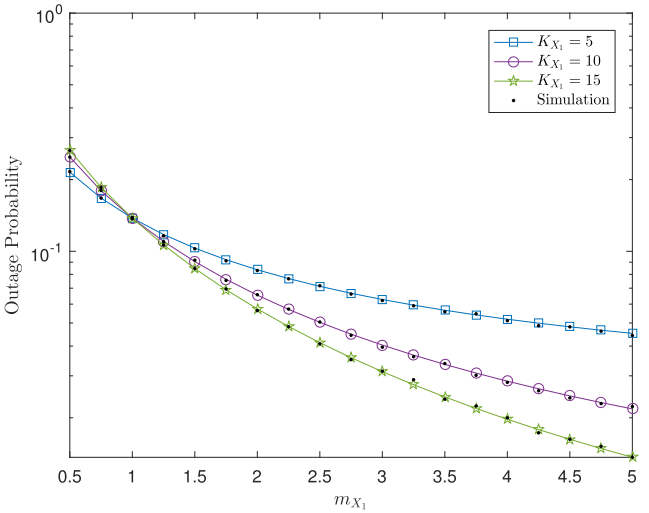

FIGURE 8. Impact of shadowing and Rician K factors on outage probability at GS for $\Omega_X = 5$dB, $\alpha_{g,g} = 1$, $\epsilon = 0.01$, $\gamma_\phi^2 = -130$dBm, $K_{Y_{si,1}} = 10$, $m_{Y_{si,1}} = 2$.

shows that having higher amounts of passive SI mitigation, i.e., smaller $m_{Y_{si,1}}$, will not further reduce outage probability at the FD-enabled GS. As SI is first mitigated at the passive SI suppression stage, residual SI is further mitigated at the active SI mitigation stage. Thus, large amounts of passive SI suppression results in less amounts of SI being mitigated at the active SI mitigation stage and vice-versa. A similar trend has also been seen in [9, Fig. 9], where higher amounts of passive SI mitigation did not result in higher SI cancellation.

Result 2: The FD-enabled GS is more reliable than the HD-GS at low signal-to-noise ratio (SNR) regimes, even in the presence of shadowing.

In Fig. 7, the HBD outage probability $\left(Pr\left(\mathcal{O}_{gs}^{HBD}\right)\right)$ and HD outage probability $\left(Pr\left(\mathcal{O}_{gs}^{HD}\right)\right)$ at GS are plotted, with the latter obtained from (32). It can be seen in Fig. 7 that even in the presence of shadowing, the FD-enabled GS achieves lower outage probability at low SNR regimes than the HD-enabled GS. The FD-enabled GS also achieves better reliability in a shadowing environment than the HD-GS operating in a non-shadowing environment at low SNR regimes.

Result 3: When severe shadowing is experienced with strong LOS component at the FD-enabled GS, reliability is diminished even when SI mitigation measures are implemented.

In Fig 8, the impact of shadowing and Rician K factors on $Pr\left(\mathcal{O}_{gs}^{HBD}\right)$, from (16), is analyzed. Interestingly, it can be seen that $Pr\left(\mathcal{O}_{gs}^{HBD}\right)$ is high when the Rician K factor is high and $m_{x_1} < 1$. Similar trends in [52, Fig. 9] have also been observed. A large Rician K factor implies that the average received power of the scattered component is low. When m is small, e.g, $m_{x_1} < 1$, severe shadowing on the LOS component is experienced. Under such circumstances, a large Rician K factor causes overall average received power to be lower than when Rician K factor is small. Also, from Corollaries 1 and 3, the Rician K factor has a positive influence on the outage probability when m is large. Therefore, the opposite is also true, i.e., a small m causes the Rician K factor to negatively impact the outage probability. Thus, the reliability of the FD-enabled GS diminishes more as the Rician K factor increases while the LOS component of the desired link ($h_{1,g}$) is obstructed, e.g., by buildings, despite the implementation of SI mitigation measures. To overcome the effect of shadowing on the desired link, relaying strategies can be considered.

TABLE 3. Error margin of the outage probability at the II and joint detectors for $\alpha_{1,2} = 0.5$.

	Ω_X = 5 dB	Ω_X = 15 dB	Ω_X = 30 dB
$m_{X_{gs}}$ = 5 (II)	2.3×10^{-5}	7.45×10^{-6}	5.35×10^{-5}
$m_{X_{gs}}$ = 15 (II)	3.6×10^{-6}	3.34×10^{-5}	2.6×10^{-5}
$m_{X_{gs}} = m_{Y_1}$ = 1000 (II)	6.91×10^{-5}	9.67×10^{-6}	8.4×10^{-6}
Rician fading (II)	3.8×10^{-4}	1.47×10^{-4}	9.46×10^{-5}
$m_{X_{gs}}$ = 5 (JD)	3.03×10^{-4}	2.79×10^{-5}	-
$m_{X_{gs}}$ = 15 (JD)	5.34×10^{-5}	8.1×10^{-7}	-
$m_{X_{gs}} = m_{Y_1}$ = 1000 (JD)	1.17×10^{-6}	-	-
Rician fading (JD)	5.23×10^{-6}	-	-

B. IMPACT OF INTER-UAV INTERFERENCE AND SHADOWING AT UAV-2

Result 4: Severe shadowing on the desired link has the equivalent impact of higher inter-UAV interference at the II detector, which results in diminished reliability.

The HBD outage probability for the II detector $\left(Pr\left(\mathcal{O}_2^{HBD(II)}\right)\right)$ at UAV-2, computed from (23), is plotted in Fig. 9a for $m_{X_{gs}} \in \{5, 15, 1000\}$ and $\alpha_{1,2} \in \{0.5, 0.7\}$. Also, $Pr\left(\mathcal{O}_2^{HBD(II)}\right)$ is plotted in Fig. 9a for the II detector over Rician fading channels using (24), where it is seen to be matching with (23) for $m_{X_{gs}} = m_{Y_1} = 1000$ and $\alpha_{1,2} \in \{0.5, 0.7\}$. For HD-UCS, $Pr\left(\mathcal{O}_2^{HD}\right)$ is plotted using (35). The error margins of the outage probability at UAV-2 are shown in Table 3.

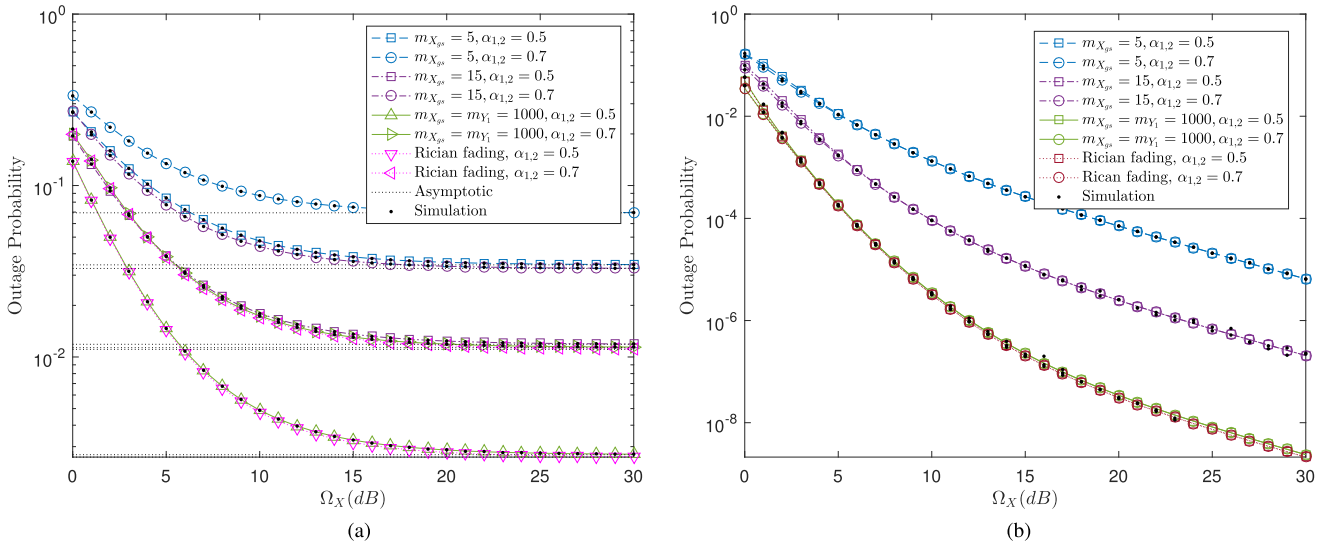

FIGURE 9. Outage probability at UAV-2 for $\alpha_{g,2} = 1$, $K_{X_{gs}} = K_{Y_1} = 15$, $m_{Y_1} = 10$. (a) Impact of shadowing on the II detector. (b) Impact of shadowing on the joint detector.

In Fig. 9a, similar observations seen in Fig. 6a are noted. Specifically, a lower $Pr\left(\mathcal{O}_2^{HBD(II)}\right)$ is attained when the desired link ($h_{g,2}$) experiences less severe shadowing than the interfering link ($h_{1,2}$), i.e., $m_{X_{gs}} > m_{Y_1}$. Also, for $m_{X_{gs}} = 5$ and $\alpha_{1,2} = 0.5$, $Pr\left(\mathcal{O}_2^{HBD(II)}\right)$ is similar to that obtained for $m_{X_{gs}} = 15$ and $\alpha_{1,2} = 0.7$. Similar observations are also made for the case of $m_{X_{gs}} = 15$ and $\alpha_{1,2} = 0.5$, and $m_{X_{gs}} = 1000$ and $\alpha_{1,2} = 0.7$. Therefore, severe shadowing on the desired link has the equivalent effect of higher inter-UAV interference levels on the received signal at the II detector. From Fig. 9a, it is apparent that both shadowing on the desired link and inter-UAV interference causes the II detector to have diminished reliability. Thus, deploying the II detector-based HBD-UCS for multi-UAV networks in urban environments results in diminished reliability. Such a limitation inadvertently places constraints on the overall Quality-of-Service (QoS) requirements for the multi-UAV network.

Result 5: Shadowing and inter-UAV interference reduces the outage probability decay rate of the joint detector at low SNR regimes.

The HBD outage probability for the joint detector $\left(Pr\left(\mathcal{O}_2^{HBD(JD)}\right)\right)$ at UAV-2, computed from (30), is plotted in Fig. 9b for $m_{X_{gs}} \in \{5, 15\}$ and $\alpha_{1,2} \in \{0.5, 0.7\}$. For reference, $Pr\left(\mathcal{O}_2^{HBD(JD)}\right)$ is plotted in Fig. 9b over Rician fading channels using (31) to reflect the outage probability at the joint detector in the absence of shadowing.

From Fig. 9b, the effect of shadowing on the joint detector is more pronounced than inter-UAV interference, especially at moderate and high SNR regimes. Since the joint detector works well in the presence of strong interference [22]–[25], it is not interference-limited at high SNR regimes. Instead, the combined effect of shadowing and inter-UAV interference reduces the outage probability decay rate at low SNR regimes. When $m_{X_{gs}} = 15$ and $\alpha_{1,2} \in \{0.5, 0.7\}$, $Pr\left(\mathcal{O}_2^{HBD(JD)}\right)$ decays more steeply then when $m_{X_{gs}} = 5$ and $\alpha_{1,2} \in \{0.5, 0.7\}$. Thus,

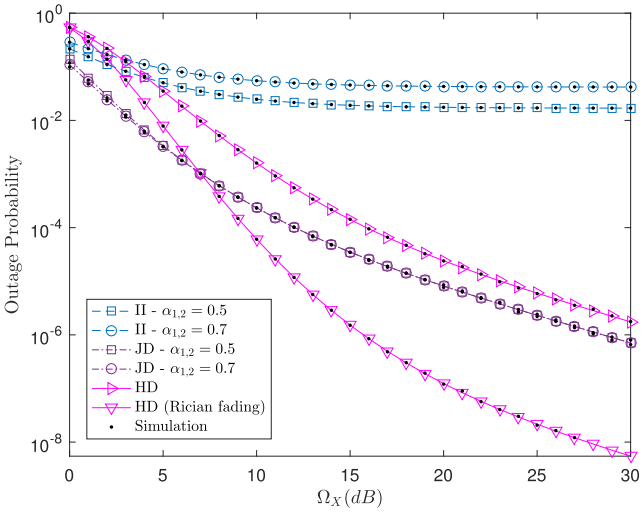

FIGURE 10. Comparison between the II and joint detectors at UAV-2 for $\alpha_{g,2} = 1$, $K_{X_{gs}} = K_{Y_1} = 15$, $m_{X_{gs}} = m_{Y_1} = 10$.

the joint detector exhibits higher reliability when $\alpha_{1,2} \to \infty$ and $m_{X_{gs}} > m_{Y_1}$. In contrast to the II detector, multi-UAV networks with joint detector-based HBD-UCS can achieve higher reliability, especially in urban environments.

Result 6: In the presence of inter-UAV interference and shadowing, the joint detector exhibits lower outage probability than the II detector and the HD-UCS at low SNR regimes.

In Fig. 10, the HBD outage probability of the II detector $\left(Pr\left(\mathcal{O}_2^{HBD(II)}\right)\right)$ and the joint detector $\left(Pr\left(\mathcal{O}_2^{HBD(JD)}\right)\right)$ are plotted. In addition, the HD-UCS outage probability at UAV-2 $\left(Pr\left(\mathcal{O}_2^{HD}\right)\right)$ is also plotted using (33). As reference, $Pr\left(\mathcal{O}_2^{HD}\right)$ in the absence of shadowing is provided using (14) by substituting $\Omega = \Omega_X \alpha_{g,2}$, $K = K_{X_{gs}}$, and $\gamma = \gamma_{th,2}^{HD}$.

From Fig. 10, outage probability trends observed for the II detector in [15, Fig. 4] are also seen in Fig. 10. Specifically, it is seen in Fig. 10 that the II detector attained lower

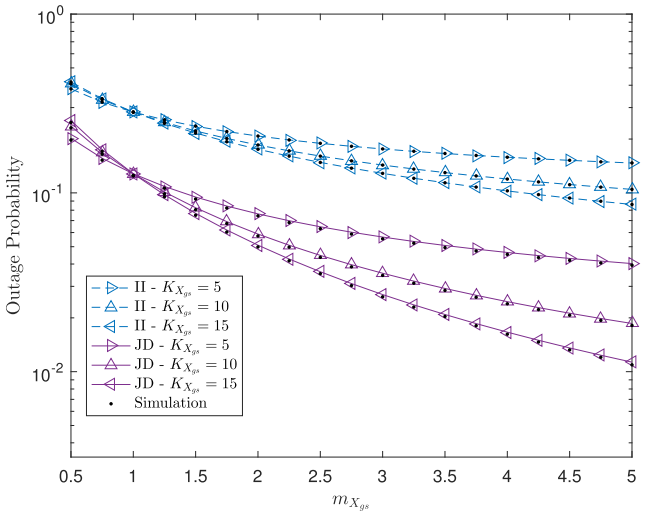

FIGURE 11. Impact of shadowing and Rician K factors on outage probability at UAV-2 for $\Omega_X = 5$dB, $\alpha_{g,2} = 1$, $\alpha_{1,2} = 0.5$, $K_{Y_1} = 10$, $m_{Y_1} = 10$.

outage probability than the HD-UCS at low SNR regimes. The same is also observed when the HD-UCS is not experiencing the effects of shadowing, i.e., HD-UCS over Rician fading channels. However, at high SNR regimes, the II detector is observed to be interference-limited due to the error floor observed in Fig. 10.

For the joint detector, the attained outage probability is less than the HD-UCS when shadowing is considered. When shadowing is not experienced at the HD-UCS, the joint detector achieves lower outage probability for $\Omega_X < 7$dB. In addition, the superiority of the joint detector over the II detector is highlighted. Therefore, the HBD-UCS shows superior reliability over HD-UCS. The joint detector clearly outperforms the II detector in terms of reliability. Thus, the former is more suitable for multi-UAV networks with high QoS requirements.

Result 7: Severe shadowing with strong LOS component has less effect on the joint detector than on the II detector.

In Fig. 11, the same observations made in Fig. 8 are noted. Thus, severe shadowing on the desired link ($h_{g,2}$) with large Rician K factor diminishes the reliability of the II and joint detectors. However, the effect is less extensive for the joint detector than the II detector since outage probability of the former is lower than the latter. As such, the superiority of the joint detector over the II detector is highlighted in severe shadowing environments, e.g., urban environments.

VI. CONCLUSION

An HBD-UCS, consisting of HD UAVs and FD GSs, is investigated as an alternative to address spectrum scarcity in UAV communications. To effectively model the underlying communication channels, Rician shadowed fading is assumed on all links to account for shadowing introduced in urban environments. To this end, an innovative mathematical framework is presented to obtain alternative closed-form representations related to both the Rician shadowed fading and the Rician fading models. Closed-form outage probability expressions for the II and the joint detectors are then obtained from the derived expressions. An extensive outage probability analysis of the HBD-UCS was conducted under various inter-UAV interference and shadowing scenarios over Rician shadowed fading channels. At the GS, the impact of shadowing on the desired link and the SI link was demonstrated. Specifically, at the GS, shadowing on the desired link impacts the outage probability considerably. On the other hand, shadowing on the SI link has negligible impact on GS outage probability. Additionally, it is also demonstrated the GS operates with lower outage probability in FD mode than in HD mode. At UAV-2, it was shown that the joint detector attains lower outage probability than the II detector and the HD-UCS. The robustness of the joint detector under severe shadowing on the desired link was also demonstrated. Thus, the superior reliability and robustness of the joint detectors makes it an ideal candidate for multi-UAV networks operating in congested urban environments. Work is in progress on designing relaying strategies and transmit power optimization for the HBD-UCS to overcome the negative effect of shadowing.

APPENDIX A
PROOF OF THEOREM 1

To begin, we note that the confluent hypergeometric function ${}_1F_1(\bullet)$ is expressed as [53]:

$$ {}_1F_1(a;b;z) = \sum_{k\geq 0} \frac{(a)_k z^k}{(b)_k k!}, \tag{36}$$

where $(a)_k = \frac{\Gamma(a+k)}{\Gamma(a)}$ is the Pochhammer symbol [35].

Since $\frac{(a)_{k+1}}{(a)_k} = a+n$ [54], and applying the identity in [44, eq. (25)] yields $\Gamma(k+a) \approx k^a \Gamma(k)$ when $k \to \infty$, then:

$$ {}_1F_1(a;1;z) = \sum_{k\geq 0} f(k), \tag{37}$$

where $f(k) = \frac{(a)_k}{\Gamma^2(k+1)} z^k$. The absolute convergence of $\sum_{k\geq 0} f(k)$ is easily proven via the D'Alembert test:

$$\begin{aligned} \lim_{k\to\infty} \frac{f(k+1)}{f(k)} &= \lim_{k\to\infty} \frac{(a+k)z}{k^2} \\ &= 0. \end{aligned} \tag{38}$$

From the Cauchy product theorem [55], [56], (7) can be expressed in truncated form, thus yielding (9):

$$\begin{aligned} f_h(x) &= \left(\sum_{n\geq 0} c(n)\right)\left(\sum_{i\geq 0} d(i)\right) \\ &\approx \sum_{n=0}^{K_{tr}} \sum_{i=0}^{n} \frac{m^m (1+K)}{\Omega (K+m)^m} \frac{(m)_i}{\Gamma^2(i+1)} \left(\frac{K(1+K)}{(K+m)\Omega}\right)^i \\ &\quad \times \left(\frac{-(1+K)}{\Omega}\right)^{n-i} \frac{x^n}{(n-i)!}, \end{aligned} \tag{39}$$

where $c(n) = \frac{m^m(1+K)}{\Omega(K+m)^m} \frac{(m)_n}{\Gamma^2(n+1)} \left(\frac{K(1+K)}{(K+m)\Omega}\right)^n x^n$, and $d(i) = \left(\frac{-(1+K)}{\Omega}\right)^i \frac{x^i}{i!}$. Thus, combining (39) with (8) yields (9) which completes the proof.

APPENDIX B
PROOF OF COROLLARY 1

To evaluate the function $\overline{a}(n, \Omega, K, m, \gamma)$ for $m \to \infty$, we first note that the asymptotic expression of $\Gamma[m+n]$, given in [44, eq. (25)], is $\Gamma[m+n] \approx m^n \Gamma[m]$, which yields $(m)_i \approx m^i$. Thereafter, substituting $(m)_i \approx m^i$ into (8) yields the following expression:

$$\begin{aligned}\overline{a}(n, \Omega, K, m, \gamma) &\approx \sum_{i=0}^{n} (-1)^{n-i} \left(\frac{m}{K+m}\right)^m \frac{K^i}{\Gamma^2(i+1)} \\ &\times \left(\frac{m}{K+m}\right)^i \left(\frac{1+K}{\Omega}\right)^{n+1} \frac{\gamma^{n+1}}{(n-i)!(n+1)}. \quad (40)\end{aligned}$$

Invoking the product rule for limits, $\lim_{m\to\infty} \overline{a}(n, \Omega, K, m, \gamma)$ can be evaluated separately:

$$\begin{aligned}\lim_{m\to\infty} \left(\frac{m}{K+m}\right)^i &= \exp\left(i \lim_{m\to\infty} \ln\left(\frac{m}{K+m}\right)\right) \\ &= 1. \quad (41)\end{aligned}$$

$$\begin{aligned}\lim_{m\to\infty} \left(\frac{m}{K+m}\right)^m &= \exp\left(\frac{\lim_{m\to\infty} \ln\left(\frac{m}{K+m}\right)}{\lim_{m\to\infty} \frac{1}{m}}\right) \\ &= \exp(-K). \quad (42)\end{aligned}$$

Combining (41) and (42) into (40) yields:

$$\begin{aligned}\widehat{a}(n, \Omega, K, \gamma) &= \lim_{m\to\infty} \overline{a}(n, \Omega, K, m, \gamma) \\ &= \sum_{i=0}^{n} \frac{(-1)^{n-i} K^i}{\Gamma^2(i+1)} \exp(-K) \left(\frac{1+K}{\Omega}\right)^{n+1} \frac{\gamma^{n+1}}{(n-i)!(n+1)}. \quad (43)\end{aligned}$$

This completes the proof.

APPENDIX C
PROOF OF COROLLARY 3

To obtain the l^{th} moment of $|h'|^2$, i.e., $E\{(|h'|^2)^l\}$, from (11), the transformation formula ${}_2F_1(a, b; c; z) = (1-z)^{c-a-b} {}_2F_1(c-a, c-b; c; z)$ [39] is invoked upon (11) to yield:

$$\begin{aligned}E\{(|h|^2)^l\} &= \left(\frac{\Omega}{1+K}\right)^l \Gamma(1+l) \left(\frac{m}{K+m}\right)^{m-1-l} \left(1+\frac{K}{m}\right)^{m-1-l} \\ &\times {}_2F_1\left(m, -l; 1; \frac{-K}{m}\right). \quad (44)\end{aligned}$$

Thereafter, $E\{(|h'|^2)^l\}$ is obtained by evaluating $\lim_{m\to\infty} E\{(|h|^2)^l\}$ with the product rule for limits:

$$\begin{aligned}\lim_{m\to\infty} \left(1+\frac{K}{m}\right)^{m-1-i} &= \exp\left(\frac{\lim_{m\to\infty} \ln\left(1+\frac{K}{m}\right)}{\lim_{m\to\infty} \frac{1}{m-1-i}}\right) \\ &= \exp(K). \quad (45)\end{aligned}$$

$$\begin{aligned}\lim_{m\to\infty} \left(\frac{m}{K+m}\right)^{m-1-i} &= \exp\left(\frac{\lim_{m\to\infty} \ln\left(\frac{m}{K+m}\right)}{\lim_{m\to\infty} \frac{1}{m-1-i}}\right) \\ &= \exp(-K). \quad (46)\end{aligned}$$

Additionally, using the asymptotic expression $\Gamma[m+n] \approx m^n \Gamma[m]$ [44, eq. (25)], yields:

$${}_2F_1\left(m, -l; 1; \frac{-K}{m}\right) \approx \sum_{n\geq 0} \frac{(-l)_n}{n!(1)_n} (-K)^n. \quad (47)$$

Therefore, combining (45), (46), and (47) into (44) leads to (15), which completes the proof.

APPENDIX D
CONVERGENCE OF (16)

It is useful to note that (16) can be expanded as:

$$\begin{aligned}Pr(\mathcal{O}_{gs}^{HBD}) &\approx \sum_{n=0}^{K_{tr}} \sum_{i=0}^{n} \sum_{l_1+l_2+l_3=n+1} (-1)^{n-i} \left(\frac{m_{X_1}}{K_{X_1}+m_{X_1}}\right)^{m_{X_1}} \\ &\times \frac{(m_{X_1})_i}{\Gamma^2(i+1)} \left(\frac{K_{X_1}}{K_{X_1}+m_{X_1}}\right)^i \left(\frac{1+K_{X_1}}{\Omega_X}\right)^{n+1} \frac{(\gamma_{th,gs}^{HBD})^{n+1}}{(n-i)!(n+1)} \\ &\times \frac{(l_1+l_2+l_3)!}{l_1!\cdot l_2!\cdot l_3!} E\{Y_{si,1}^{l_1}\} E\{Y_{si,2}^{l_2}\} \\ &\approx \sum_{n=0}^{K_{tr}} \sum_{i=0}^{n} \sum_{l_1+l_2+l_3=n+1} \Xi(n, i, l_1, l_2, l_3). \quad (48)\end{aligned}$$

Taking the D'Alembert test, it is easily shown that:

$$\begin{aligned}\lim_{n\to\infty} \frac{|\Xi(n+1, i, l_1, l_2, l_3)|}{|\Xi(n, i, l_1, l_2, l_3)|} &\overset{(a)}{=} \lim_{n\to\infty} \left(\frac{1+K_{X_1}}{\Omega_X}\right)\left(\frac{n+1}{n+2}\right)\left(\frac{\gamma_{th,gs}^{HBD}}{n}\right) = 0, \quad (49)\end{aligned}$$

where (a) is obtained using the identity $\Gamma[m+n] \approx m^n \Gamma[m]$ [44, eq. (25)]. Therefore, (16) is absolutely convergent. This completes the proof.

APPENDIX E
PROOF OF COROLLARY 5

We begin by first proving (21). Starting from (16), the outage probability expression can be written as:

$$\begin{aligned}Pr(\mathcal{O}_{gs}^{HBD}) &\approx \sum_{n=0}^{K_{tr}} \sum_{l_1+l_2+l_3=n+1} \overline{a}(n, 1, K_{X_1}, m_{X_1}, \gamma_{th,gs}^{HBD}) \\ &\times \frac{(n+1)!}{l_1!\cdot l_2!\cdot l_3!} M\{Y_{si,1}^{l_1}\} M\{Y_{si,2}^{l_2}\} (\Omega_X)^{l_1+l_2-n-1}. \quad (50)\end{aligned}$$

To obtain the asymptotic outage probability at the GS, one will need to evaluate (50) as $\Omega_X \to \infty$. However, it is useful to note that $\lim_{\Omega_X\to\infty} (\Omega_X)^{l_1+l_2-n-1} = 0$ when $l_1+l_2<n+1$, i.e., $l_3 > 0$. On the other hand, $\lim_{\Omega_X\to\infty} (\Omega_X)^{l_1+l_2-n-1} = 1$ when $l_1+l_2 = n+1$, i.e., $l_3 = 0$. Thus, evaluating (50) for multinomial index $l_1+l_2 = n+1$ yields the asymptotic outage probability expression in (21). The same technique is also used to obtain (22). This completes the proof.

APPENDIX F
PROOF OF THEOREM 6

A. OUTAGE PROBABILITY DERIVATION

Before evaluating the closed-form outage probability expression for the joint detector $\left(Pr\left(\mathcal{O}_2^{HBD(JD)}\right)\right)$, it is useful to first obtain the PDFs of X_{gs} and Y_1. From (9), the PDFs of X_{gs} and Y_1 are given in (51) and (52), respectively:

$$f_{X_{gs}}(x) \approx \sum_{n=0}^{K_{tr}} \overline{a}\left(n, \Omega_X \alpha_{g,2}, K_{X_{gs}}, m_{X_{gs}}, 1\right)(n+1)x^n. \quad (51)$$

$$f_{Y_1}(y) \approx \sum_{n=0}^{K_{tr}} \overline{a}\left(n, \Omega_X \alpha_{1,2}, K_{Y_1}, m_{Y_1}, 1\right)(n+1)y^n. \quad (52)$$

Then, $Pr\left(\mathcal{O}_2^{HBD(JD)}\right)$ is obtained from [57, eq. (17)] as:

$$\begin{aligned} &Pr\left(\mathcal{O}_2^{HBD(JD)}\right) \\ &\quad = Pr\left\{\mathcal{O}_{JD}^1\right\} + Pr\left\{\mathcal{O}_{JD}^2\right\} \\ &\quad = F_{X_{gs}}\left(\gamma_{th,2}^{HBD}\right) + \int_{\gamma_{th,2}^{HBD}}^{b_1} f_{X_{gs}}(x)\left[F_{Y_1}\left(b_2 - x\right)\right. \\ &\qquad \left. - F_{Y_1}\left(\frac{x}{\gamma_{th,2}^{HBD}} - 1\right)\right]dx, \end{aligned} \quad (53)$$

where $\mathcal{O}_{JD}^1$ and $\mathcal{O}_{JD}^2$ are defined in (28) and (29), respectively, and both b_1 and b_2 are defined in (30). The functions $F_{X_{gs}}(\bullet)$ and $F_{Y_1}(\bullet)$ are the CDFs of X_{gs} and Y_1, respectively, obtainable from (10). To simplify the integral on the right hand side (RHS) of (53), we note that $\left(b_2 - x\right)^{n+1} - \left(\frac{x}{\gamma_{th,2}^{HBD}} - 1\right)^{n+1} = (-1)^{n+1}\sum_{k=0}^{n+1}\binom{n+1}{k}[(-b_2)^{n+1-k} - (-\gamma_{th,2}^{HBD})^{-k}]x^k$, and thus:

$$\begin{aligned} &F_{Y_1}\left(b_2 - x\right) - F_{Y_1}\left(\frac{x}{\gamma_{th,2}^{HBD}} - 1\right) \\ &\quad \approx \sum_{n=0}^{K_{tr}}\sum_{k=0}^{n+1} \overline{a}\left(n, \Omega_X \alpha_{1,2}, K_{Y_1}, m_{Y_1}, 1\right)\binom{n+1}{k} \\ &\qquad \times[(-b_2)^{n+1-k} - (-\gamma_{th,2}^{HBD})^{-k}]x^k. \end{aligned} \quad (54)$$

Let $c(n) = \sum_{k=0}^{n+1} \overline{a}\left(n, \Omega_X \alpha_{1,2}, K_{Y_1}, m_{Y_1}, 1\right)\binom{n+1}{k}[(-b_2)^{n+1-k} - (-\gamma_{th,2}^{HBD})^{-k}]x^k$ and $d(n) = \overline{a}\left(n, \Omega_X \alpha_{g,2}, K_{X_{gs}}, m_{X_{gs}}, 1\right)(n+1)x^n$. Then, applying the Cauchy product theorem onto the integral in (53) yields [55], [56]:

$$\begin{aligned} &\int_{\gamma_{th,2}^{HBD}}^{b_1} f_{X_{gs}}(x)\left[F_{Y_1}\left(b_2 - x\right) - F_{Y_1}\left(\frac{x}{\gamma_{th,2}^{HBD}} - 1\right)\right]dx \\ &\approx \int_{\gamma_{th,2}^{HBD}}^{b_1} \left(\sum_{n=0}^{K_{tr}} c(n)\right)\left(\sum_{q=0}^{K_{tr}} d(q)\right)dx \\ &\approx \int_{\gamma_{th,2}^{HBD}}^{b_1} \sum_{n=0}^{K_{tr}}\sum_{q=0}^{n} c(q)d(n-q)dx \end{aligned} \quad (55)$$

$$\begin{aligned} &\approx \sum_{n=0}^{K_{tr}}\sum_{q=0}^{n}\sum_{k=0}^{q+1} \overline{a}\left(q, \Omega_X \alpha_{1,2}, K_{Y_1}, m_{Y_1}, 1\right) \\ &\quad \times \overline{a}\left(n-q, \Omega_X \alpha_{g,2}, K_{X_{gs}}, m_{X_{gs}}, 1\right)(n+1)\binom{q+1}{k}(-1)^{q+1} \\ &\quad \times G_1\left(q, k, b_2, \gamma_{th,2}^{HBD}\right)\frac{G_2\left(k+n-q, b_1, \gamma_{th,2}^{HBD}\right)}{k+n-q+1}, \end{aligned} \quad (56)$$

where $G_1\left(q, k, b_2, \gamma_{th,2}^{HBD}\right)$ and $G_2\left(k+n-q+1, b_1, \gamma_{th,2}^{HBD}\right)$ are defined in (30). It should be pointed out that (56) is obtained by interchanging the summation and integration in (55), i.e., term-wise integration [39], which is valid for $\gamma_{th,2}^{HBD} \le x \le b_1$. Substituting (56) into (53) yields the closed-form outage probability expression for $Pr\left(\mathcal{O}_2^{HBD(JD)}\right)$ in (30) which completes the proof.

B. CONVERGENCE OF (30)

We start by expanding the joint detector outage probability expression in (30) as:

$$\begin{aligned} &Pr\left(\mathcal{O}_2^{HBD(JD)}\right) \\ &\quad \approx \sum_{n=0}^{K_{tr}}\sum_{i=0}^{n}(-1)^{n-i}\left(\frac{m_{X_{gs}}}{K_{X_{gs}} + m_{X_{gs}}}\right)^{m_{X_{gs}}}\frac{(m_{X_{gs}})_i}{\Gamma^2(i+1)} \\ &\qquad \times\left(\frac{K_{X_{gs}}}{K_{X_{gs}} + m_{X_{gs}}}\right)^{i}\left(\frac{1+K_{X_{gs}}}{\Omega_X \alpha_{g,2}}\right)^{n+1}\frac{\left(\gamma_{th,2}^{HBD}\right)^{n+1}}{(n-i)!(n+1)} \\ &\qquad + \sum_{n=0}^{K_{tr}}\sum_{q=0}^{n}\sum_{k=0}^{q+1}\sum_{s=0}^{q}\sum_{z=0}^{n-q}\left(\frac{m_{Y_1}}{K_{Y_1} + m_{Y_1}}\right)^{m_{Y_1}}\frac{(m_{Y_1})_s}{\Gamma^2(s+1)} \\ &\qquad \times\left(\frac{K_{Y_1}}{K_{Y_1} + m_{Y_1}}\right)^{s}\left(\frac{1+K_{Y_1}}{\Omega_X \alpha_{1,2}}\right)^{q+1}\frac{(-1)^{q-s}}{(q-s)!(q+1)} \\ &\qquad \times\left(\frac{m_{X_{gs}}}{K_{X_{gs}} + m_{X_{gs}}}\right)^{m_{X_{gs}}}\frac{(m_{X_{gs}})_z}{\Gamma^2(z+1)} \\ &\qquad \times\left(\frac{K_{X_{gs}}}{K_{X_{gs}} + m_{X_{gs}}}\right)^{z}\left(\frac{1+K_{X_{gs}}}{\Omega_X \alpha_{g,2}}\right)^{n-q+1} \\ &\qquad \times\frac{(-1)^{n-q-z}(n+1)\binom{q+1}{k}(-1)^{q+1}}{(n-q-z)!(n-q+1)} \\ &\qquad \times G_1\left(q, k, b_2, \gamma_{th,2}^{HBD}\right)\frac{G_2\left(k+n-q+1, b_1, \gamma_{th,2}^{HBD}\right)}{k+n-q+1} \\ &\quad \approx \sum_{n=0}^{K_{tr}}\sum_{i=0}^{n}\Theta(n,i) \\ &\qquad + \sum_{n=0}^{K_{tr}}\sum_{q=0}^{n}\sum_{k=0}^{q+1}\sum_{s=0}^{q}\sum_{z=0}^{n-q}\Delta(n,q,k,s,z). \end{aligned} \quad (57)$$

For the first term in (57), applying the D'Alembert test yields:

$$\begin{aligned} \lim_{n\to\infty}\frac{|\Theta(n+1,i)|}{|\Theta(n,i)|} &\overset{(a)}{=} \lim_{n\to\infty}\gamma_{th,2}^{HBD}\left(\frac{1+K_{X_{gs}}}{\Omega_X \alpha_{g,2}}\right)\left(\frac{n+1}{n+2}\right)\left(\frac{1}{n}\right) \\ &= 0, \end{aligned} \quad (58)$$

where (a) results from the identity $\Gamma[m+n] \approx m^n\Gamma[m]$ [44, eq. (25)]. Therefore, the first term in (57) is absolutely convergent.

For the second term in (57), applying the D'Alembert test yields:

$$\begin{aligned}
&\lim_{n\to\infty}\frac{|\Delta(n+1,q,k,s,z)|}{|\Delta(n,q,k,s,z)|}\\
&\quad\overset{(a)}{=}\lim_{n\to\infty}\frac{(n-q+1)(n+2)(k+n-q+1)}{(n-q+2)(n+1)(k+n-q+2)}\left(\frac{1}{n}\right)\\
&\qquad\times\frac{G_2\left(k+n-q+2,b_1,\gamma_{th,2}^{HBD}\right)}{G_2\left(k+n-q+1,b_1,\gamma_{th,2}^{HBD}\right)}\\
&\quad\overset{(b)}{=}\lim_{n\to\infty}\frac{(n-q+1)(n+2)(k+n-q+1)}{(n-q+2)(n+1)(k+n-q+2)}\\
&\qquad\times\left(\frac{\gamma_{th,2}^{HBD}2^{R_1^{HBD}}}{n}\right)=0,
\end{aligned}\tag{59}$$

where (a) is due to the identity $\Gamma[m+n] \approx m^n\Gamma[m]$ [44, eq. (25)], and (b) is due to the fact that:

$$\begin{aligned}
&\lim_{n\to\infty}\frac{G_2\left(k+n-q+2,b_1,\gamma_{th,2}^{HBD}\right)}{G_2\left(k+n-q+1,b_1,\gamma_{th,2}^{HBD}\right)}\\
&=\lim_{n\to\infty}\frac{\left(\gamma_{th,2}^{HBD}\right)^{k+n-q+2}\left[\left(2^{R_1^{HBD}}\right)^{k+n-q+2}-1\right]}{\left(\gamma_{th,2}^{HBD}\right)^{k+n-q+1}\left[\left(2^{R_1^{HBD}}\right)^{k+n-q+1}-1\right]}\\
&=\gamma_{th,2}^{HBD}2^{R_1^{HBD}}.
\end{aligned}\tag{60}$$

As such, (59) shows that the second term in (57) is absolutely convergent. Therefore, (30) is also absolutely convergent. This completes the proof.

APPENDIX G
PROOF OF COROLLARY 9

Starting with the case of the joint detector over Rician shadowed fading channels, the outage probability expression from (30) can be expressed as:

$$\begin{aligned}
&Pr\left(\mathcal{O}_2^{HBD(JD)}\right)\\
&\approx\sum_{n=0}^{K_{tr}}\overline{a}\left(n,\alpha_{g,2},K_{X_{gs}},m_{X_{gs}},\gamma_{th,2}^{HBD}\right)(\Omega_X)^{-n-1}\\
&\quad+\sum_{n=0}^{K_{tr}}\sum_{q=0}^{n}\sum_{k=0}^{q+1}\overline{a}\left(q,\alpha_{1,2},K_{Y_1},m_{Y_1},1\right)\\
&\quad\times\overline{a}\left(n-q,\alpha_{g,2},K_{X_{gs}},m_{X_{gs}},1\right)(n+1)\binom{q+1}{k}(-1)^{q+1}\\
&\quad\times G_1\left(q,k,b_2,\gamma_{th,2}^{HBD}\right)\frac{G_2\left(k+n-q,b_1,\gamma_{th,2}^{HBD}\right)}{k+n-q+1}(\Omega_X)^{-n-2}.
\end{aligned}\tag{61}$$

From (61), it can be seen that $\lim_{\Omega_X\to\infty} Pr\left(\mathcal{O}_2^{HBD(JD)}\right) = 0$, since $\lim_{\Omega_X\to\infty}(\Omega_X)^{-n-1} = 0$ and $\lim_{\Omega_X\to\infty}(\Omega_X)^{-n-2} = 0$. As such, the joint detector achieves zero outage probability at asymptotic SNR regimes. For the case of the joint detector over Rician fading channels, repeating the above steps also yield zero outage probability at asymptotic SNR regimes. This completes the proof.

ACKNOWLEDGMENT

This research is jointly funded by Airbus Singapore Pte Ltd and the Singapore Economic Development Board (EDB).

REFERENCES

[1] T. Andre, K. A. Hummel, A. P. Schoellig, E. Yanmaz, M. Asadpour, C. Bettstetter, P. Grippa, H. Hellwagner, S. Sand, and S. Zhang, "Application-driven design of aerial communication networks," *IEEE Commun. Mag.*, vol. 52, no. 5, pp. 129–137, May 2014.

[2] N. H. Motlagh, M. Bagaa, and T. Taleb, "UAV selection for a UAV-based integrative IoT platform," in *Proc. IEEE Global Commun. Conf. (GLOBECOM)*, Washington, DC, USA, Dec. 2016, pp. 1–6.

[3] J.-J. Wang, C.-X. Jiang, Z. Han, Y. Ren, R. G. Maunder, and L. Hanzo, "Taking drones to the next level: Cooperative distributed unmanned-aerial-vehicular networks for small and mini drones," *IEEE Veh. Technol. Mag.*, vol. 12, no. 3, pp. 73–82, Sep. 2017.

[4] S. Sekander, H. Tabassum, and E. Hossain, "Multi-tier drone architecture for 5G/B5G cellular networks: Challenges, trends, and prospects," *IEEE Commun. Mag.*, vol. 56, no. 3, pp. 96–103, Mar. 2018.

[5] D. W. Matolak and R. Sun, "Air–ground channel characterization for unmanned aircraft systems—Part III: The suburban and near-urban environments," *IEEE Trans. Veh. Technol.*, vol. 66, no. 8, pp. 6607–6618, Aug. 2017.

[6] D. W. Matolak and R. Sun, "Unmanned aircraft systems: Air-ground channel characterization for future applications," *IEEE Veh. Technol. Mag.*, vol. 10, no. 2, pp. 79–85, Jun. 2015.

[7] T. Z. H. Ernest, A. S. Madhukumar, R. P. Sirigina, and A. K. Krishna, "A hybrid-duplex system with joint detection for interference-limited UAV communications," *IEEE Trans. Veh. Technol.*, vol. 68, no. 1, pp. 335–348, Jan. 2019.

[8] T. Z. H. Ernest, A. S. Madhukumar, R. P. Sirigina, and A. K. Krishna, "Outage analysis and finite SNR diversity-multiplexing tradeoff of hybrid-duplex systems for aeronautical communications," *IEEE Trans. Wireless Commun.*, vol. 18, no. 4, pp. 2299–2313, Apr. 2019.

[9] A. Sahai, G. Patel, C. Dick, and A. Sabharwal, "On the impact of phase noise on active cancelation in wireless full-duplex," *IEEE Trans. Veh. Technol.*, vol. 62, no. 9, pp. 4494–4510, Nov. 2013.

[10] E. Ahmed and A. M. Eltawil, "All-digital self-interference cancellation technique for full-duplex systems," *IEEE Trans. Wireless Commun.*, vol. 14, no. 7, pp. 3519–3532, Jul. 2015.

[11] A. Sabharwal, P. Schniter, D. Guo, D. W. Bliss, S. Rangarajan, and R. Wichman, "In-band full-duplex wireless: Challenges and opportunities," *IEEE J. Sel. Areas Commun.*, vol. 32, no. 9, pp. 1637–1652, Sep. 2014.

[12] D. Korpi, T. Riihonen, V. Syrjälä, L. Anttila, M. Valkama, and R. Wichman, "Full-duplex transceiver system calculations: Analysis of ADC and linearity challenges," *IEEE Trans. Wireless Commun.*, vol. 13, no. 7, pp. 3821–3836, Jul. 2014.

[13] R. Li, A. Masmoudi, and T. Le-Ngoc, "Self-interference cancellation with nonlinearity and phase-noise suppression in full-duplex systems," *IEEE Trans. Veh. Technol.*, vol. 67, no. 3, pp. 2118–2129, Mar. 2018.

[14] T. Z. H. Ernest, R. P. Sirigina, A. K. Krishna, and A. S. Madhukumar, "On the performance analysis of hybrid-duplex systems for aeronautical communications," in *Proc. IEEE 87th Veh. Technol. Conf. (VTC Spring)*, Porto, Portugal, Jun. 2018, pp. 1–5.

[15] T. Z. H. Ernest, A. Madhukumar, R. P. Sirigina, and A. K. Krishna, "Hybrid-duplex systems for UAV communications under rician shadowed fading," in *Proc. IEEE 88th Veh. Technol. Conf. (VTC Fall)*, Chicago, IL, USA, Aug. 2018, pp. 1–5.

[16] T. Z. H. Ernest, A. S. Madhukumar, R. P. Sirigina, and A. K. Krishna, "Hybrid-duplex based control and non-payload communication systems for UAVs: An outage analysis," in *Proc. IEEE/AIAA 37th Digit. Avionics Syst. Conf. (DASC)*, Sep. 2018, pp. 1–6.

[17] M. Mohammadi, H. A. Suraweera, Y. Cao, I. Krikidis, and C. Tellambura, "Full-duplex radio for uplink/downlink wireless access with spatially random nodes," *IEEE Trans. Commun.*, vol. 63, no. 12, pp. 5250–5266, Dec. 2015.

[18] X. Yue, Y. Liu, S. Kang, A. Nallanathan, and Z. Ding, "Exploiting full/half-duplex user relaying in NOMA systems," *IEEE Trans. Commun.*, vol. 66, no. 2, pp. 560–575, Feb. 2017.

[19] L. Qu, J. He, and C. Assi, "Understanding the benefits of successive interference cancellation in multi-rate multi-hop wireless networks," *IEEE Trans. Commun.*, vol. 62, no. 7, pp. 2465–2477, Jul. 2014.

[20] S. P. Weber, J. G. Andrews, X. Yang, and G. de Veciana, "Transmission capacity of wireless ad hoc networks with successive interference cancellation," *IEEE Trans. Inf. Theory*, vol. 53, no. 8, pp. 2799–2814, Aug. 2007.

[21] V. S. Annapureddy and V. V. Veeravalli, "Gaussian interference networks: Sum capacity in the low-interference regime and new outer bounds on the capacity region," *IEEE Trans. Inf. Theory*, vol. 55, no. 7, pp. 3032–3050, Jul. 2009.

[22] D. Zahavi and R. Dabora, "On cooperation and interference in the weak interference regime," *IEEE Trans. Inf. Theory*, vol. 63, no. 6, pp. 3894–3922, Jun. 2017.

[23] G. Zhou, W. Xu, and G. Bauch, "Is MAC joint decoding optimal for interference channels?" in *Proc. 81st Veh. Technol. Conf. (VTC Spring)*, Glasgow, U.K., 2015, pp. 1–5.

[24] I. Shubhi and Y. Sanada, "Joint turbo decoding for overloaded MIMO-OFDM systems," *IEEE Trans. Veh. Technol.*, vol. 66, no. 1, pp. 433–442, Jan. 2017.

[25] J. Blomer and N. Jindal, "Transmission capacity of wireless ad hoc networks: Successive interference cancellation vs. joint detection," in *Proc. IEEE Int. Conf. Commun. (ICC)*, Dresden, Germany, Jun. 2009, pp. 1–5.

[26] D. W. Matolak, "Air-ground channels & models: Comprehensive review and considerations for unmanned aircraft systems," in *Proc. IEEE Aerosp. Conf.*, Big Sky, MT, USA, Mar. 2012, pp. 1–17.

[27] A. Al-Hourani, S. Kandeepan, and S. Lardner, "Optimal LAP altitude for maximum coverage," *IEEE Wireless Commun. Lett.*, vol. 3, no. 6, pp. 569–572, Dec. 2014.

[28] R. Sun and D. W. Matolak, "Air–ground channel characterization for unmanned aircraft systems Part II: Hilly and mountainous settings," *IEEE Trans. Veh. Technol.*, vol. 66, no. 3, pp. 1913–1925, Mar. 2017.

[29] N. Goddemeier and C. Wietfeld, "Investigation of air-to-air channel characteristics and a UAV specific extension to the rice model," in *Proc. IEEE Globecom Workshops (GC Wkshps)*, San Diego, CA, USA, Dec. 2015, pp. 1–5.

[30] X. Yuan, Z. Feng, W. Xu, W. Ni, J. A. Zhang, Z. Wei, and R. P. Liu, "Capacity analysis of UAV communications: Cases of random trajectories," *IEEE Trans. Veh. Technol.*, vol. 67, no. 8, pp. 7564–7576, Aug. 2018.

[31] L. Zeng, X. Cheng, C.-X. Wang, and X. Yin, "A 3D geometry-based stochastic channel model for UAV-MIMO channels," in *Proc. IEEE Wireless Commun. Netw. Conf. (WCNC)*, San Francisco, CA, USA, Mar. 2017, pp. 1–5.

[32] K. Jin, X. Cheng, X. Ge, and X. Yin, "Three dimensional modeling and space-time correlation for UAV channels," in *Proc. IEEE 85th Veh. Technol. Conf. (VTC Spring)*, Sydney, NSW, Australia, Jun. 2017, pp. 1–5.

[33] H. Jiang, Z. Zhang, and G. Gui, "Three-dimensional non-stationary wideband geometry-based UAV channel model for A2G communication environments," *IEEE Access*, vol. 7, pp. 26116–26122, 2019.

[34] H. Jiang, Z. Zhang, L. Wu, and J. Dang, "Three-dimensional geometry-based UAV-MIMO channel modeling for A2G communication environments," *IEEE Commun. Lett.*, vol. 22, no. 7, pp. 1438–1441, Jul. 2018.

[35] Y. J. Chun, S. L. Cotton, H. S. Dhillon, F. J. Lopez-Martinez, J. F. Paris, and S. K. Yoo, "A comprehensive analysis of 5G heterogeneous cellular systems operating over $\kappa - \mu$ shadowed fading channels," *IEEE Trans. Wireless Commun.*, vol. 16, no. 11, pp. 6995–7010, Nov. 2017.

[36] J. F. Paris, "Statistical characterization of $\kappa - \mu$ shadowed fading," *IEEE Trans. Veh. Technol.*, vol. 63, no. 2, pp. 518–526, Feb. 2014.

[37] J. Zhang, X. Chen, K. P. Peppas, X. Li, and Y. Liu, "On high-order capacity statistics of spectrum aggregation systems over $\kappa - \mu$ and $\kappa - \mu$ shadowed fading channels," *IEEE Trans. Commun.*, vol. 65, no. 2, pp. 935–944, Feb. 2017.

[38] X. Li, J. Li, L. Li, J. Jin, J. Zhang, and D. Zhang, "Effective rate of MISO systems over $\kappa - \mu$ shadowed fading channels," *IEEE Access*, vol. 5, pp. 10605–10611, Jun. 2017.

[39] I. S. Gradshteĭn and I. M. Ryžik, *Table of Integrals, Series, and Products*. New York, NY, USA: Academic, 2014.

[40] S. Kumar, "Approximate outage probability and capacity for $\kappa - \mu$ shadowed fading," *IEEE Wireless Commun. Lett.*, vol. 4, no. 3, pp. 301–304, Jun. 2015.

[41] A. Al-Hourani and K. Gomez, "Modeling cellular-to-UAV path-loss for suburban environments," *IEEE Wireless Commun. Lett.*, vol. 7, no. 1, pp. 82–85, Feb. 2018.

[42] R. Amorim, H. Nguyen, P. Mogensen, I. Z. Kovács, J. Wigard, and T. B. Sørensen, "Radio channel modeling for UAV communication over cellular networks," *IEEE Wireless Commun. Lett.*, vol. 6, no. 4, pp. 514–517, Aug. 2017.

[43] A. Abdi, W. C. Lau, M.-S. Alouini, and M. Kaveh, "A new simple model for land mobile satellite channels: First- and second-order statistics," *IEEE Trans. Wireless Commun.*, vol. 2, no. 3, pp. 519–528, May 2003.

[44] N. B. Rached, A. Kammoun, M.-S. Alouini, and R. Tempone, "A unified moment-based approach for the evaluation of the outage probability with noise and interference," *IEEE Trans. Wireless Commun.*, vol. 16, no. 2, pp. 1012–1023, Feb. 2017.

[45] N. H. Motlagh, T. Taleb, and O. Arouk, "Low-altitude unmanned aerial vehicles-based Internet of Things services: Comprehensive survey and future perspectives," *IEEE Internet Things J.*, vol. 3, no. 6, pp. 899–922, Dec. 2016.

[46] C. Yao, L. Song, and Y. Li, "X-duplex radios: Flexible switching between full-duplex and half-duplex," *IEEE Wireless Commun. Lett.*, vol. 7, no. 1, pp. 94–97, Feb. 2018.

[47] N. Zlatanov, E. Sippel, V. Jamali, and R. Schober, "Capacity of the Gaussian two-hop full-duplex relay channel with residual self-interference," *IEEE Trans. Commun.*, vol. 65, no. 3, pp. 1005–1021, Mar. 2017.

[48] P. C. Sofotasios, M. K. Fikadu, S. Muhaidat, Q. Cui, G. K. Karagiannidis, and M. Valkama, "Full-duplex regenerative relaying and energy-efficiency optimization over generalized asymmetric fading channels," *IEEE Trans. Wireless Commun.*, vol. 16, no. 5, pp. 3232–3251, May 2017.

[49] A. Bennatan, S. Shamai (Shitz), and A. R. Calderbank, "Soft-decoding-based strategies for relay and interference channels: Analysis and achievable rates using LDPC codes," *IEEE Trans. Inf. Theory*, vol. 60, no. 4, pp. 1977–2009, Apr. 2014.

[50] B. Bandemer, A. El Gamal, and Y.-H. Kim, "Simultaneous nonunique decoding is rate-optimal," in *Proc. 50th Annu. Allerton Conf. Commun., Control, Comput. (Allerton)*, Monticello, IL, USA, 2012, pp. 9–16.

[51] W. Nam, D. Bai, J. Lee, and I. Kang, "Advanced interference management for 5G cellular networks," *IEEE Commun. Mag.*, vol. 52, no. 5, pp. 52–60, May 2014.

[52] S. Kumar and S. Kalyani, "Outage probability and rate for $\kappa - \mu$ shadowed fading in interference limited scenario," *IEEE Trans. Wireless Commun.*, vol. 16, no. 12, pp. 8289–8304, Dec. 2017.

[53] S. Parthasarathy and R. K. Ganti, "Coverage analysis in downlink poisson cellular network with $\kappa - \mu$ shadowed fading," *IEEE Wireless Commun. Lett.*, vol. 6, no. 1, pp. 10–13, Feb. 2017.

[54] G. Boros and V. Moll, *Irresistible Integrals: Symbolics, Analysis and Experiments in the Evaluation of Integrals*. Cambridge, U.K.: Cambridge Univ. Press, 2004.

[55] S. András, A. Baricz, and Y. Sun, "The generalized Marcum Q-function: An orthogonal polynomial approach," *Acta Univ. Sapientiae Math.*, vol. 3, no. 1, pp. 60–76, 2011.

[56] H. Amann, J. Escher, S. Levy, and M. Cargo, *Analysis*, vol. 3. Basel, Switzerland: Birkhäuser Verlag, 2005.

[57] R. Narasimhan, "Individual outage rate regions for fading multiple access channels," in *Proc. ISIT*, Nice, France, 2007, pp. 1571–1575.

TAN ZHENG HUI ERNEST received the B.Eng. in computer engineering (First Class Honours) from Nanyang Technological University (NTU), in 2015. He is currently pursuing the Ph.D. degree in computer engineering with NTU. He is currently a Research Engineer with Airbus Singapore Private Limited. His current research interests include the evaluation of interference management in aeronautical communications and the performance analysis of unmanned aerial vehicle communications in fifth generation (5G) networks.

A. S. MADHUKUMAR (M'96–SM'02) received the B.Tech. degree from the College of Engineering, Trivandrum, India, the M.Tech. degree from the Cochin University of Science and Technology, Cochin, India, and the Ph.D. degree from the Indian Institute of Technology Madras, Chennai, India.

He is currently an Associate Professor with the School of Computer Science and Engineering, Nanyang Technological University, Singapore. He was involved in communications and signal processing research with the Centre for Development of Advanced Computing, Government of India, and the Institute for Infocomm Research (previously known as the Centre for Wireless Communications), Singapore. His current research interests include heterogeneous networks, cooperative radio systems for mobile multihop networks, algorithms and architectures of cognitive radios, new modulation and multiple access schemes, and advanced signal processing algorithms for communication systems. He is involved in a number of funded research projects, organizing international conferences, and a permanent Reviewer for many internationally reputed journals and conferences. He has authored or coauthored more than 250 referred international conferences and journal papers.

RAJENDRA PRASAD SIRIGINA received the B.Tech. degree in electronics and communications engineering from the Gokaraju Rangaraju Institute of Engineering and Technology, Jawaharlal Nehru Technological University, Hyderabad, India, in 2002, the M.Tech. degree in signal processing from the Indian Institute of Technology Guwahati, Guwahati, India, in 2007, and the Ph.D. degree from the school of computer engineering (SCE), Nanyang Technological University (NTU), Singapore, in 2015.

He is currently a Research Fellow with the School of Computer Science and Engineering, NTU, Singapore. He was a Lecturer for 3 years in Hyderabad, India. He taught courses related to communication theory for undergraduate students. He was a Deputy Manager with the Reliance Technology Innovation Center, Reliance Communications, Navimumbai, India, for 2 years. He was also a Research Associate with NTU for approximately 2 years. His current research interests include interference management in 5G and satellite networks.

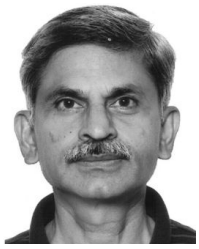

ANOOP KUMAR KRISHNA (SM'03) He obtained the M.Tech. degree in digital electronics from the Cochin University of Science and Technology, India, in 1989 and the M.Sc. degree in Physics with Specialization in Applied Electronics from the University of Kerala, India, in 1986 and the Ph.D. degree in electronics and communication engineering from the National Institute of Technology (NIT) Tiruchirappalli, India, in 1996. He has also received a Graduate Certificate in Intellectual Property (GCIP) from the National University of Singapore, in May 2007. He has over 25 years of experience in Industry and Academics. He joined Airbus in Research and Technology Centre, Singapore, in July 2007. He has worked on various wireless and wired communication systems and technology development for different business units of Airbus, including various collaborative research projects with different research institutes and Universities. He is currently leading the R&T activities in the Skyways project. He has also served as TPC member for various conferences and as a Reviewer for Journal and conference articles. He has about 50 research publications in journals and conferences of international repute and in the form of granted patents.